Journal of Solid State Chemistry 270 (2019) 618–635

Contents lists available at ScienceDirect

Journal of Solid State Chemistry

journal homepage: www.elsevier.com/locate/jssc

Structural variations, relationships and properties of M_2B metal borides

Abishek K. Iyer[1], Yuemei Zhang[1], Jan P. Scheifers, Boniface P.T. Fokwa*

Chemistry Department, University of California, Riverside, CA 92521, United States

ARTICLE INFO

Keywords:
Metal borides
M_2B
Trigonal prism
$CeCo_3B_2$-type
Boron fragments
Boron chains
Magnetism
Superconductivity
Catalysis

ABSTRACT

Metal borides represent a class of materials with a large variety of crystal structures, yet their physical and catalytic properties are overwhelmingly understudied. In this review, we present the structural variations, relationships and properties of metal borides with a metal-to-boron ratio (M:B) of 2:1, which have over 130 known phases (from binaries to quaternaries) that crystallize with 21 structure types. While most of these structure types contain isolated boron atoms only, B–B-bonds (d(B–B) < 2.0 Å) are observed in nine of them (less than half). Even though several coordination environments for boron atoms are found, the trigonal prismatic coordination (CN = 6(+3), present in seventeen structure types) is by far the most common followed by the square anti-prismatic coordination (CN = 8). These trigonal prisms can be undistorted like in the $CeCo_3B_2$-type, where boron consequently resides in the exact center, but also distorted prisms are found for example in the Co_2Si-type. Stronger distortions like in the $ZrCo_3B_2$-type can lead to the formation of short B–B-bonds (d(B–B) < 2.0 Å). When B-centered trigonal prisms share common rectangular faces, bonding between neighboring boron occurs. Ni_3ZnB_2 and $Ti_{1+x}Rh_{2-x+y}Ir_{3-y}B_3$ are examples with zigzag B_4 fragments and in $Ti_{1+x}Os_{2-x}RuB_2$ trigonal planar B_4 fragments are found. In the case of the MoAlB-type the rectangular faces are shared leading to a zigzag B-chain.

Except for the anti-MoS_2-type (Pt_2B, existence is still debated), the unit cell length of the short axis in these structures is always close to 3.0 Å, which corresponds to the height of a typical B[M_6] prism. In the case of URu_3B_2 and $ZrCo_3B_2$ the short axis is doubled respectively tripled due to their superstructure in comparison to the related $CeCo_3B_2$-type.

Even though interesting magnetic and superconducting properties have been reported in many phases (especially in the $CeCo_3B_2$-type) as well as some fascinating catalytic behaviors (such as in $CuAl_2$-type phases), more must be done in the future to capitalize on the structural diversity from this 2:1 borides composition space.

1. Introduction

Structural characterization of borides has resulted in many structures exhibiting different boron substructures. In the last decade many general and specialized reviews have been published on the structure-property relationship of these compounds [1–6]. Kiessling classified binary metal borides based on their M:B ratio [7]. With over 150 different boride structure types, segregation based on the M:B ratio can help design and discover new borides [8]. Compounds with a high M:B-ratio (high metal content) exhibit crystal structures with isolated boron atoms, for example Re_3B (M:B = 3) [9] or Rh_7B_3 (M:B ≈ 2.33) [10]. Boron linkages are observed with decreasing metal contents such as boron dumbbells which occur for example in Cr_5B_3 (M:B ≈ 1.6) [11], and boron zigzag chains are found in the structure of FeB (M:B = 1) [12], 2D boron layers in MgB_2(M:B = 0.5) [13] while 3D B-substructures can be observed in CaB_6 (M:B = 0.16) [14] and YB_{66} (M:B = 0.015) [15]. However, multinary borides can expand the composition space even more, with phases such as $Nd_2Fe_{14}B$ exhibiting the highest M:B ratio to date (M:B = 16) [16]. Such a huge compositional diversity predestines this compound class to achieving nearly any imaginable physical property. Yet, their difficult synthesis and thus the lack of attractiveness to the scientific community make studying new materials or the properties of known ones a big challenge. Nevertheless, many borides have found applications, such as $Nd_2Fe_{14}B$ which is the best permanent magnet [17,18], MgB_2 which is a the first metallic superconductor with T_c > 30 K (39 K) [13], and YB_{66} used as monochromator for soft synchrotron radiation [15]. Recently some binary metal borides have been studied as potential catalysts for hydrogen evolution reactions (HER) and possible hydrogenation of C=O bond [19,20].

* Corresponding author.
E-mail address: bfokwa@ucr.edu (B.P.T. Fokwa).
[1] Co-first authors.

https://doi.org/10.1016/j.jssc.2018.12.014
Received 4 September 2018; Received in revised form 4 December 2018; Accepted 11 December 2018
Available online 13 December 2018
0022-4596/

Table 1
Structure types of compounds with an M:B ratio of 2:1.

Type	Spacegroup	Pearson symbol	Boron units	CN(B)	CN(Shape)	Related
$CeCo_3B_2$	*P6/mmm*	hP6	–	9	tricapped trigonal prismatic[a]	
$ErIr_3B_2$	*C2/m*	mC12	–	9	tricapped trigonal prismatic[a]	$CeCo_3B_2$
$ZrCo_3B_2$	$R\bar{3}$	hR18	B_2 pairs	9	trigonal prismatic[b]	$CeCo_3B_2$
$(Nd_{0.71}Rh_{0.29})Rh_3B_2$	$P\bar{6}2m$	hP6	–	9	tricapped trigonal prismatic[a]	$CeCo_3B_2$
URu_3B_2	$P\bar{3}$	hP48	–	9	tricapped trigonal prismatic[a]	$CeCo_3B_2$
$CuAl_2$	*I4/mcm*	tI12	–	8	square antiprismatic	
Mg_2Cu	*Fddd*	oF48	–	8	square antiprismatic	$CuAl_2$
CuIrB	*Fdd2*	oF48	–	7	irregular polyhedra	$CaRh_2B_2$ LiIrB
$Cu_2Ir_4B_3$	*Cmcm*	oC20	–	6	trigonal prismatic	$ZnIr_4B_3$
Pt_2B	*C2/m*	mC24	–	6	trigonal prismatic	
Co_2Si	*Pnma*	oP12	–	9	tricapped trigonal prismatic[a]	
ZrNiAl	$P\bar{6}2m$	hP9	–	9	tricapped trigonal prismatic	
TiNiSi	*Pnma*	oP12	–	9	tricapped trigonal prismatic[a]	Co_2Si
NbCoB	*Pmmn*	oP30	–	9	tricapped trigonal prismatic[a]	ZrNiAl TiNiSi
$Ti_{1+x}Os_{2-x}RuB_2$	$P\bar{6}2m$	hP18	B_4 trigonal planar unit	6,7,9	trigonal prismatic[c]	
$Ti_{1+x}Rh_{2-x+y}Ir_{3-y}B_3$	*Pbam*	oP36	B_4 zigzag unit	6,9	trigonal prismatic[c]	$Ti_{1+x}Os_{2-x}RuB_2$
NbRuB	*Pmma*	oP16	B_2 dumbbells	6	trigonal prismatic[c]	
HT-$Nb_{1+x}Os_{1-x}B$	*Pnma*	oP12	zigzag chains	6	trigonal prismatic[c]	
Ni_3ZnB_2	*C2/m*	mC24	B_4 zigzag unit	9	tricapped trigonal prismatic[a]	
MoAlB	*Cmcm*	oC12	zigzag chains	9	tricapped trigonal prismatic[a]	

[a] Distorted trigonal prism
[b] Two faces capes by Zr and one short B–B contact leading to boron pairs
[c] uncapped (CN6), one face capped (CN7), three faces capped (CN9)

This review exclusively focuses on the very versatile ratio M:B = 2:1, which shows a very diverse pool of structures containing isolated boron atoms and/or several types of B-B linkages. About 130 compounds have been reported with this M:B ratio and more than 50% of them have individual B atoms, most of which crystallize in the prolific $CeCo_3B_2$-type structure and its derivatives [8]. However, in the last decade, there has been an increasing number of more complex structures which contain (i) boron linkages such as trigonal planar B_4-fragments in $Ti_{1+x}Os_{2-x}RuB_2$-type [21], trans zigzag B_4 fragments in $Ti_{1+x}Rh_{2-x+y}Ir_{3-y}B_3$-type [22], B_2 dumbbells in NbRuB and (ii) new modifications such as LT-NbOsB (zigzag B_4) [23] and HT-NbOsB (isolated boron atoms and an infinite boron chain) [24]. These examples nicely illustrate that the M:B = 2:1 ratio might just be an ideal playground to understand the structural diversity in borides. Table 1 describes all reported structure types with the ratio M:B = 2:1. When available, we also report on the different physical and catalytic properties studied for this group of metal borides.

2. Compounds containing mainly isolated boron atoms

2.1. $CeCo_3B_2$-type and its distorted variants

Over 40 ternary borides crystallizing in the $CeCo_3B_2$-type have been reported, which makes it the most abundant among metal borides with M:B = 2:1 [25] while another 20 ternary borides have been reported to crystallize in the $ErCo_3B_2$ structure type, a distorted variant of the $CeCo_3B_2$-type [26]. Additionally, there are other variants: $Nd_xRh_3B_2$ [27], URu_3B_2 [28], $ZrCo_3B_2$ [29] which have been characterized only through powder X-ray diffraction.

2.1.1. $CeCo_3B_2$-type: The most prolific among all M_2B structures

The $CeCo_3B_2$-type is made up of corner-sharing trigonal prisms of the transition metal centered by isolated boron atoms. This structural arrangement is observed in all other above-mentioned variants other than the $ZrIr_3B_2$-type where the distortion in the structure results in B-B dumbbells. The following series have been synthesized successfully: *RE*Co_3B_2 (*RE* = Sc, Y, Ce, Sm, Gd-Lu, U) [30,31]; *RE*Ir_3B_2 (*RE* = La, Pr, Th, U) [32,33]; *RE*Rh_3B_2 (*RE* = La, Ce, Pr, Nd, Sm, Eu, Gd) [32]; *RE*Ru_3B_2 (*RE* = Y, La, Ce, Pr, Nd, Sm, Gd-Lu, Th) [32]. Furthermore (Lu,U)Os_3B_2 [32] and UFe_3B_2 [34,35] have been reported to crystallize with the $CeCo_3B_2$-type structure.

$CeCo_3B_2$ crystallizes in space group *P6/mmm* (Pearson symbol: *hP6*) [25] and it is best described as an ordered variant of the $CaCu_5$-type [36]. Cerium is located on the calcium site, and the two Cu-sites have Co on the 3*g* site and boron located on 2*c* in comparison to the $CaCu_5$-type structure. The structure of $CeCo_3B_2$, shown in Fig. 1a

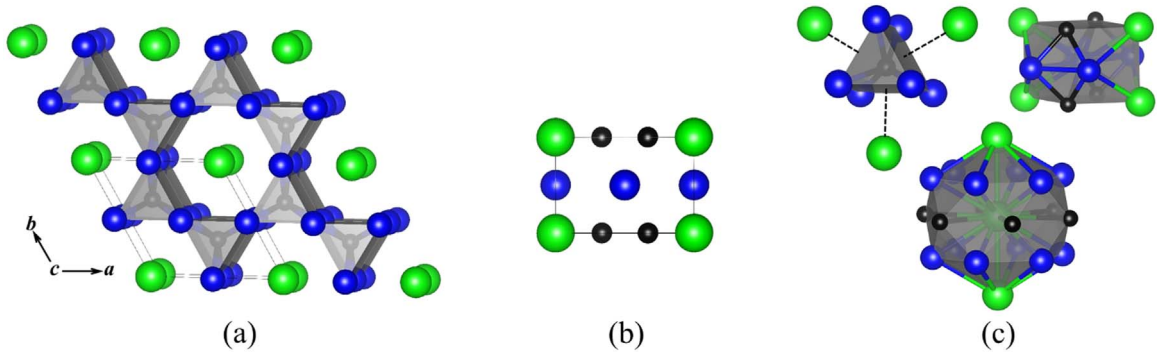

Fig. 1. (a) Structure of $CeCo_3B_2$ (own type), view on the *ab*-plane. (b) View on the *ac*-plane. (c) Coordination polyhedra around boron, cobalt and cerium. Blue, green and black spheres represent Co, Ce and B atoms, respectively. (For interpretation of the references to color in this figure legend, the reader is referred to the web version of this article).

contains two alternating layers along the *c*-axis: the layer at $z = ½$ is exclusively occupied with Co-atoms, while that at $z = 0$ holds the boron and cerium atoms (Fig. 1b). The boron atoms are coordinated by nine metal atoms, forming a boron-centered tricapped trigonal prism, $B[Co_6Ce_3]$ (Fig. 1c). Thus, the $CeCo_3B_2$-type is one of many structures containing the frequently found $B[M_6]$ unit. The Co prisms are connected by sharing three edges resulting in Kegomé nets and hexagonal voids which hold the larger rare earth elements. The relatively short B–Co contacts $d(B–Co) = 2.11$ Å inside the trigonal prisms indicate strong bonding interactions. Cobalt is coordinated by 12 atoms forming a four-capped tetragonal prism $Co[Ce_4Co_4B_4]$ (Fig. 1c), while cerium is coordinated by 20 atoms forming a fully capped hexagonal prism, $Ce[Ce_2Co_{12}B_6]$ (Fig. 1c). The presence of large cavities incorporating rare-earth atoms points to possible distortion of this structure type depending on the sizes of the substituted elements, implying new variants. The following sections discuss these structural variants.

2.1.2. The $ErIr_3B_2$-type: A monoclinic variant of $CeCo_3B_2$-type

In 1980, Ku et al. reported about a new structure, the $ErIr_3B_2$-type with space group *C*2/*m* (Pearson symbol *mC*12) [26]. The coordination environments of boron and the metal atoms in $ErIr_3B_2$-type are very similar to those of the $CeCo_3B_2$-type structure. In fact, the $ErIr_3B_2$-type is a distorted variant of the $CeCo_3B_2$-type. Even though the powder patterns of compounds adopting this structure are very similar to those of the hexagonal $CeCo_3B_2$-type, most of the reflections split and were indexed in a monoclinic cell with $a_m \approx a_h$, $b_m \approx (3)^{1/2}a_h$, $c_m \approx c_h$ and $\beta \geq 90°$ (Fig. 2). Fig. 3 gives an overview of ternary compounds adopting the $ErIr_3B_2$- or the $CeCo_3B_2$-type structures. Over 20 compounds adopting the $ErIr_3B_2$-type are known, such as $RERh_3B_2$ (*RE* = Y, Tb-Lu, Pu) and $REIr_3B_2$ (*RE* = Sc, Y, Ce, Nd, Sm, Gd-Lu, Pu) series. While there was ambiguity over the two structure types ($ErIr_3B_2$- and the $CeCo_3B_2$-type) for $RERh_3B_2$, successful crystal growth of $ErRh_3B_2$ using Cu flux by Shishido et al. confirmed that it crystallizes in the $ErIr_3B_2$ structure type [37]. However, Ye et al. in a later paper observed severe twinning in the *ab*-plane, quantitative intensity measurements were unsuccessful and consequently the crystal structure could not be solved in the super-lattice for $ErRh_3B_2$, $GdRh_3B_2$ and $TmRh_3B_2$. Recently Kubota et al. reported that the compound $CeIr_3B_2$ undergoes a structural transition from monoclinic to hexagonal at ~395 K which indicates the close relation between the two structures as shown in Fig. 2 [38]. These studies suggest the superstructure could be a universal problem concerning the borides of the $RERh_3B_2$ system as explained by Ye et al. who also claim that partial boron vacancies and modulations of the Rh or B atoms due to self-accommodation to the pseudo hexagonal lattice are the reason [39].

2.1.3. Other closely related $CeCo_3B_2$-type structural variants

The $(Nd_{0.71}Rh_{0.29})Rh_3B_2$-, $ErIr_3B_2$-, and URu_3B_2-type structures are other distorted variants closely related to the $CeCo_3B_2$-type structure.

From a structural point of view, the $(Nd_{0.71}Rh_{0.29})Rh_3B_2$-type is the closest to the $CeCo_3B_2$-type. The structure can be described in space group $P\bar{6}2m$, the only difference to the $CeCo_3B_2$-type being the x parameter of 0.51 for the Rh site instead of the ideal ½ found for Co [27].

The URu_3B_2-type is a superstructure of the $CeCo_3B_2$-type with a doubling of the initial *a*-, *b*- and *c* -lattice parameters [28]. The structural distortion originates from the fact that some of the ruthenium atoms building the Ru-layer are slightly shifted away from their ideal positions (Fig. 4).

2.1.4. $ZrCo_3B_2$-type: A B_2-containing variant of $CeCo_3B_2$-type

In the $ZrCo_3B_2$-type, distortions of the $B[M_6]$ trigonal prisms are observed. Stadelmaier et al. had previously suggested that $ZrCo_3B_2$ crystallized in the $CeCo_3B_2$-type structure. However, Voroshilov et al. reinvestigated the structures of $HfCo_3B_2$ and $ZrCo_3B_2$ and discovered that both compounds crystallize in a more complex structure, space group $R\bar{3}$ (Pearson symbol *hR*18) which corresponds to another distorted variant of the $CeCo_3B_2$-type [29]. The crystal structure is shown in Fig. 5a. The B atoms are considerably displaced from the prism center which leads to the formation of B_2-dumbbells with short boron contacts: $d(B–B) = 1.70$ Å. Along the [001] direction, the different layers in the unit cell are still present, however those consisting of Co atoms are strongly puckered (Fig. 5). Compared to the $CeCo_3B_2$-type, the unit cell is twelve-fold with a tripled *c*-axis. The Zr/B layer is also puckered but not in the same magnitude as the Co layer.

2.1.5. Physical properties of $CeCo_3B_2$-type and its variants

Many rare-earth or transition metal borides have been investigated for superconductivity, magnetic and magnetocaloric properties. In the $CeCo_3B_2$ structure type superconductivity was reported up to 4.6 K for all compounds with non-magnetic rare-earth metals as shown in the Table 2 published by Ku et al., while for those containing rare-earth with partially filled 4*f*-orbitals no superconductivity above 1.2 K was found. Magnetic ordering at temperatures above 45 K has been observed for compounds with half-filled *f*-orbitals: $SmRh_3B_2$ is a canted antiferromagnet having intrinsic magnetic hardness with a coercive force of 50 kOe at 4.2 K [40]. Some of $RECo_3B_2$ series are paramagnetic and others are ferromagnetically ordered at low temperatures [41]. $GdCo_3B_2$ undergoes two magnetic transitions at 54 K and 160 K [42]. The magnetic properties of $TbCo_3B_2$ compound show

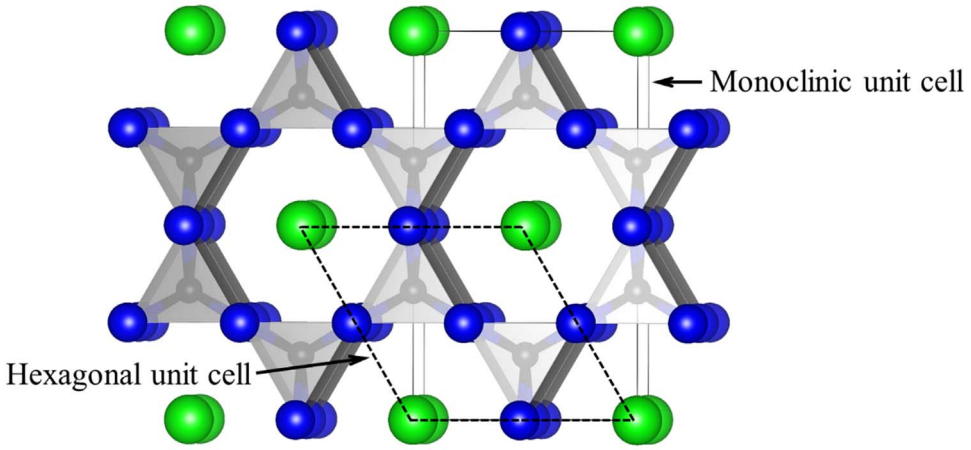

Fig. 2. Relatioship between the unit cells of $ErIr_3B_2$- and $CeCo_3B_2$-types. Blue, green and black spheres represent Ir, Er and B atoms, respectively. (For interpretation of the references to color in this figure legend, the reader is referred to the web version of this article.)

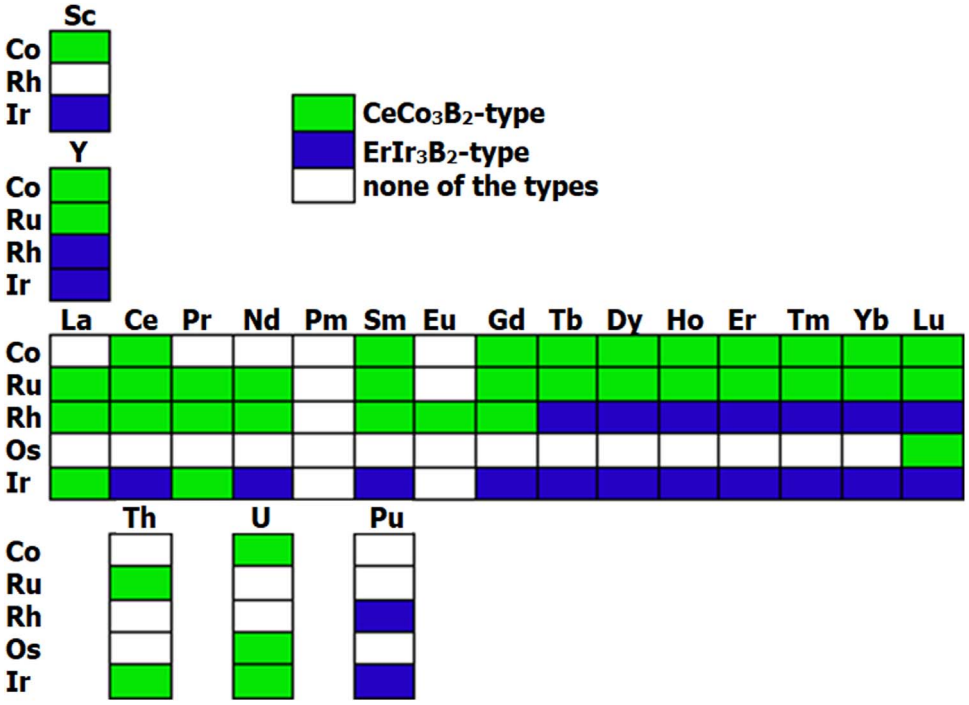

Fig. 3. Overview of ternary compounds crystallizing in the $CeCo_3B_2$- and the $ErIr_3B_2$-type structures.

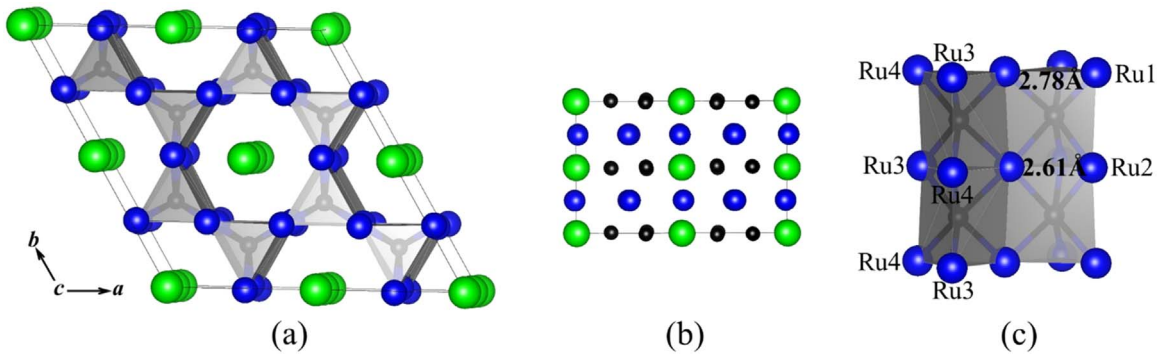

Fig. 4. (a) Crystal structure of URu_3B_2. (b) View on the ac-plane. (c) Two types of distortion of trigonal prisms around boron atoms, B[Ru1Ru2$Ru3_2$$Ru4_2$] (left) and B[$Ru1_3$$Ru2_3$] (right).

some contrasting results, as Dubman et al. have described two magnetic transitions [43] whereas only one transition temperature was observed by Li et al. [42]. Large magnetocaloric effect (MCE) has also been found in $GdCo_3B_2$, $TbCo_3B_2$, $DyCo_3B_2$ and $HoCo_3B_2$ [42,44–46]. As suggested by Ku et al. [32] its appears that the superconductivity may be influenced by the local magnetic moment of the transition

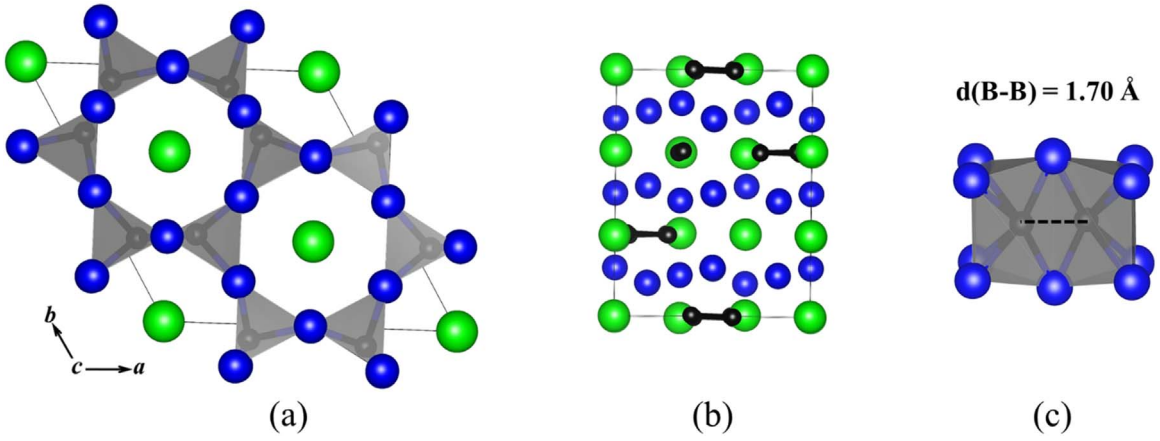

Fig. 5. (a) Crystal structure of $ZrCo_3B_2$ (own type) (b) View on the ac-plane. (c) B_2-unit and coordination polyhedron around boron. Blue, green and black spheres represent Co, Zr and B atoms, respectively. (For interpretation of the references to color in this figure legend, the reader is referred to the web version of this article).

Table 2
Superconducting temperatures reported in the $CeCo_3B_2$-type and its variant structures [32].

Compound	T_c (K)
$LaRh_3B_2$	2.82–2.60
$(Y_{0.5}La_{0.5})Rh_3B_2$	1.88–1.56
$LuOs_3B_2$	4.62–4.45
$(Lu_{0.5}Th_{0.5})Os_3B_2$	4.14–3.84
$LaIr_3B_2$	1.65–1.38
$ThIr_3B_2$	2.09–1.90

metals but the lack of any transition metal clusterin $CeCo_3B_2$-type structure might be a reason for the observed low T_c. This work additionally lays an interesting claim that with atomic % higher than 11% of RE , superconductivity is not commonly observed.

2.2. The $CuAl_2$-type and its variant Mg_2Cu

2.2.1. $CuAl_2$-type: Structure, solid solutions, magnetic and catalytic properties

With more than 30 reported compounds, the $CuAl_2$-type is another common structure type observed in metal borides with M:B = 2:1 [8]. $CuAl_2$ crystalizes in space group *I*4/*mcm* (Pearson symbol *tl*12). In these borides, boron atoms sit on the Cu site, coordinated in a square anti-prismatic manner by eight metal atoms. B[M_8] square anti-prisms stack along the *c*-axis to form B[M_4] rod by sharing their square faces (Fig. 6a). The B[M_4] rods connects in *a*, *b*-directions by sharing edges with 4 other B[M_4] rods (Fig. 6b).

Table 3 summarizes the list of binary compounds reported in the $CuAl_2$-type structure. The existence of Ti_2B and Cr_2B however is doubtful, as two possible sets of lattice parameters resulting from

Table 3
Compounds crystallizing in the Cu_2Al and Mg_2Cu-type structures. "doubtful" compositions.

Compound	Structure type	*a* (Å)	*c* (Å)	*V* (Å^3)	References
"Ti_2B"	Cu_2Al	6.11	4.56	170.2	[47,95]
"Cr_2B"	Mg_2Cu	5.19	4.32	116.0	[11,48,58,59]
Mn_2B	Mg_2Cu	5.15	4.21	111.5	[48,61]
Fe_2B	Cu_2Al	5.12	4.18	109.2	[12,48,96,97]
Co_2B	Cu_2Al	5.01	4.21	105.6	[12,48]
Ni_2B	Cu_2Al	4.98	4.24	105.1	[48,97]
Mo_2B	Cu_2Al	5.55	4.74	145.5	[48]
Ta_2B	Cu_2Al	5.78	4.86	162.4	[48]
W_2B	Cu_2Al	5.57	4.75	147.1	[48,97]

two different interpretations of the powder patterns were reported [47]. Cr_2B has been discussed in greater detail in the Mg_2Cu-type structure (see below). Starting from the binary phases, great efforts have been made to partially substitute the M atoms in the binary compounds to study the possible solid solution. Due to the large number of compounds, we want to point out some well documented systems. Havinga et al. published a series of four papers dealing with binary and ternary compounds crystalizing in the $CuAl_2$-type [48–51]. The investigated ternary boride systems are $Ta_{2-x}Mo_xB$, $Ta_{2-x}W_xB$, $Mo_{2-x}Re_xB$ and $W_{2-x}Re_xB$. In general, solid solutions were found for systems where both end members crystalize in the $CuAl_2$-type, however in $Ta_{2-x}Mo_xB$ complete miscibility was not observed due to the large differences in the unit cell volume of the end members. In systems where only one end member has the $CuAl_2$ structure the solid-solubility is naturally limited e.g. $Mo_{2-x}Re_xB$ and $W_{2-x}Re_xB$. Kuz'min et al. found that in the system $(Fe_{1-x}Co_x)_2B$ when x is between 0.1 and 0.5, especially for the composition $(Fe_{0.7}Co_{0.3})_2B$ its magnetic hardness is comparable to that

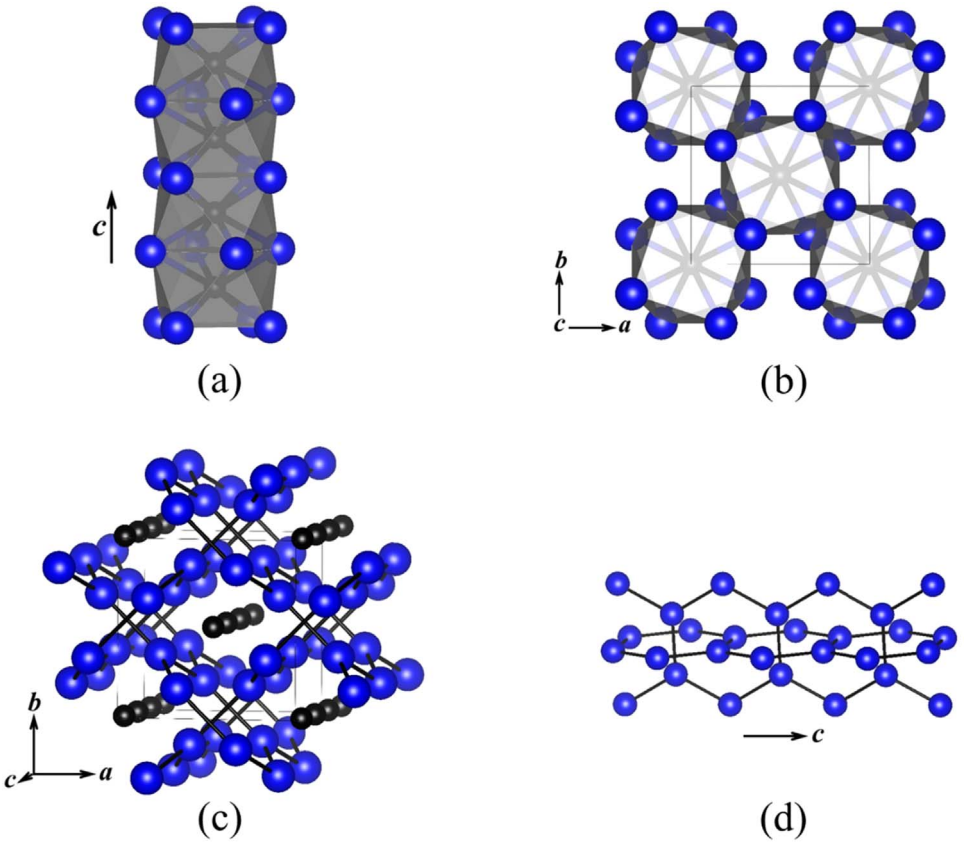

Fig. 6. The $CuAl_2$-type. (a) B[M_4] rod in the M_2B compounds (M = Mn-Ni, Mo, Ta, W); (b) Perspective views of the crystal structure of M_2B along the *c* direction; (c) and (d) Metal-metal honeycomb structure. Blue and black spheres represent M and B atoms, respectively. (For interpretation of the references to color in this figure legend, the reader is referred to the web version of this article).

of commercial Barium ferrite [52]. In 2015, Skokov et al. reported that doping by 2.5 at% of Re on the Fe/Co site shows a 50% increase of the magnetocrystalline anisotropy energy if compared to its parent compound $(Fe_{0.7}Co_{0.3})_2B$ [53].

Interestingly, Kalyon et al. found that nanoscale Co_2B is an active catalyst toward liquid phase hydrogenation of citral by a preferential hydrogenation of C=O bonds [54]. The same group recently reported on nanoscale $(Fe_{0.7}Co_{0.3})_2B$ as a high-performance electrocatalyst for the oxygen evolution reaction in alkaline solution that can challenge traditional but expensive noble metal oxide catalysts such as IrO_2 and RuO_2 [54,55]. However, we have found that polycrystalline Mo_2B is far less active for hydrogen evolution reaction (HER) than other molybdenum borides in acidic conditions [20] while Massa et al. also reported less HER activity for crystalline Co_2B in alkaline solution if compared with the amorphous and supported catalysts [56].

2.2.2. The Mg_2Cu-type: An orthorhombic distorted $CuAl_2$-type

Mg_2Cu crystallizes in space group *Fddd* (Pearson symbol *oF*48). It contains the similar $B[M_4]$ rods as seen in the $CuAl_2$ structure type (see Fig. 6a), but with slightly distorted $B[M_8]$ square anti-prisms. Both $CuAl_2$- and Mg_2Cu-type structures can be described by using the concept of rod packing [57]. The $CuAl_2$-type is described as a simple tetragonal packing of rods (see Fig. 7a). In the Mg_2Cu-type structure, two layers of $B[M_4]$ rods are present with one running in the [011] direction in one layer and another running in the [01 $\bar{1}$] direction in another layer (see Fig. 7b). Within the layer, each $B[M_4]$ rod connects with two other $B[M_4]$ rods by sharing their edges. The two different layers alternate along the *a*-direction to form the 3D crystal structure.

Bimetallic borides of 3d metals Ti, Cr and Mn are reported to crystallize in the Mg_2Cu-type structure. As mentioned above, Cr_2B and Mn_2B may also crystallize in the $CuAl_2$-type structure. Cr_2B is well characterized [11,48,58–60] in the Mg_2Cu-type structure. In the case of manganese, both the tetragonal (*t*-Mn_2B, $CuAl_2$-type) and the orthorhombic (*o*-Mn_2B, Mg_2Cu-type) variants are reported. *o*-Mn_2B was first reported as "Mn_4B" by Kiessling et al. [7]. Due to the low accuracy of earlier investigations, Tergenius et al. reinvestigated the crystal structure of "Mn_4B" by means of single-crystal X-ray diffraction. The orthorhombic cell was confirmed, and the refinement led to the final composition Mn_2B. Furthermore, Tergenius et al. stated that both phases form directly from arc melts and no transformation between them could be observed, not even after an extensive heating treatment, neither was it possible to obtain a two-phase sample containing both *o*-Mn_2B and *t*-Mn_2B [61].

2.3. The layer-like structure types LiIrB, CuIrB and $Cu_2Ir_4B_3$

In 1994, Jung et al. investigated the ternary systems (Li, Cu, Pd)-Ir-B. They found that the compounds CuIrB and PdIrB are isostructural, crystallize in the orthorhombic system (space group: *Fdd*2*;* Pearson symbol: oF48) and can be related to the LiIrB structure (space group *Fddd*) [62].

This CuIrB structure contains solely isolated boron atoms (see Fig. 8a). The coordination polyhedra around boron consist of 4 iridium and 3 copper atoms which form a capped distorted trigonal prism, $B[Ir_4Cu_3]$. The boron-iridium contacts with d(B–Ir) = 2.05 – 2.18 Å are rather short and indicate strong bonding. In fact, connecting these bonds lead to IrB_4-tetrahedra which are edge-sharing and build a 3D network with empty 1D channels incorporating the Cu atoms. This structural description is supported by the fact that the boron-copper contacts, d(B–Cu) = 2.20 – 2.40 Å, are slightly larger than the sum of the metallic radii, implying weak bonding. A behavior expected from copper because it usually forms boron-rich compounds and preferably acts as a metal with a closed d-shell showing weak bonding to boron. The atomic environment of the metal atoms is rather complex: Copper is coordinated by 13 atoms $Cu[B_3Ir_5Cu_5]$, and iridium by 12 $Ir[B_4Cu_5Ir_3]$ (see Fig. 8b). Homoatomic contacts for copper are greater than the sum of the metallic radii d(Cu–Cu) = 2.73 – 3.04 Å and in the case of iridium shorter contacts d(Ir–Ir) = 2.72 – 2.73 Å are found, indicating stronger bonding interactions than for copper. Cu-Ir contacts range from 2.70 up to 3.00 Å and exceed the sum of their metallic radii.

The structure of CuIrB can be viewed as a distorted variant of LiIrB [62]. Starting from LiIrB, the lithium atoms are replaced by Cu atoms, which results in a very similar but distorted structure (see Fig. 8a and c). The Ir/B framework is quite similar in both CuIrB and LiIrB. Looking at the Cu/Ir and Li/Ir layers (see Fig. 8a and c), the distortion of CuIrB in comparison to LiIrB is obvious: The Cu chains in CuIrB are shifted in comparison to the Ir chains.

In 1999 Jung et al. reported a compound with the formula $Cu_2Ir_4B_3$ [63] crystallizing in the orthorhombic crystal system (space group: *Cmcm;* Pearson symbol: oC20). The structure of $Cu_2Ir_4B_3$ is shown in Fig. 9a. Parallel to the *c*-axis Ir/B sheets and double layers of Cu-atoms are found and they alternate along the *b*-direction. The Ir/B sheets are built up by three rows of $B[Ir_6]$ prisms as shown in Fig. 9b. The $[Ir_6]$ prisms of the central row are centered by boron but the refinement of the occupancy for the boron site (B2 site) resulted in a site occupation factor of approx. 50%. The two outer rows are formed by $B[Ir_6]$-prisms stacked on top of each other and parallel to the *c*-axis (Fig. 9b). The iridium-boron contacts d(Ir–B) = 2.15 – 2.25 Å are rather short and indicate strong bonding. Ir-Ir contacts are slightly larger than in the element d(Ir–Ir) = 2.81–2.92 Å but can still be considered to have significant bonding interactions. Surprisingly, there exist rather short Cu–Cu contacts in $Cu_2Ir_4B_3$ with d(Cu–Cu) = 2.46 Å. On the other hand, the Cu–Ir contacts d(Cu–Ir) = 2.70 Å are fairly long, leading to weak interactions, which could explain the layer-like nature of $Cu_2Ir_4B_3$.

The authors also discussed the probability for the occurrence of B–B bonds: In fact, the occupancy for the B2- site is refined to 0.48

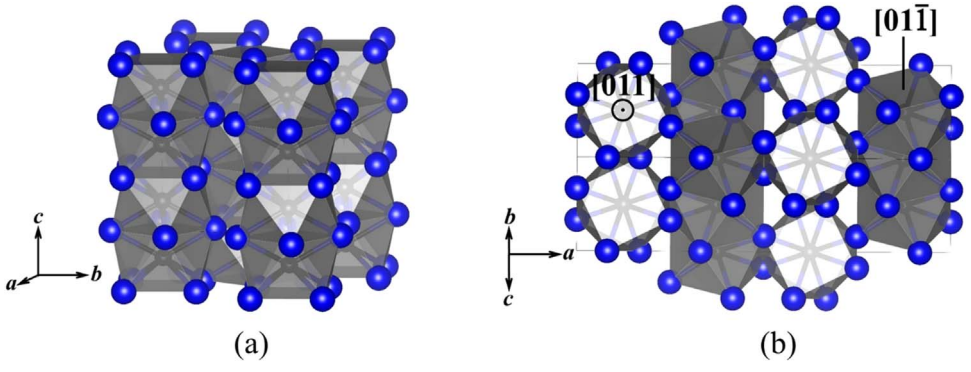

Fig. 7. $B[M_4]$ Rods packing in (a) the $CuAl_2$- and (b) the Mg_2Cu-type structures. Blue and black spheres represent M and B atoms, respectively. (For interpretation of the references to color in this figure legend, the reader is referred to the web version of this article).

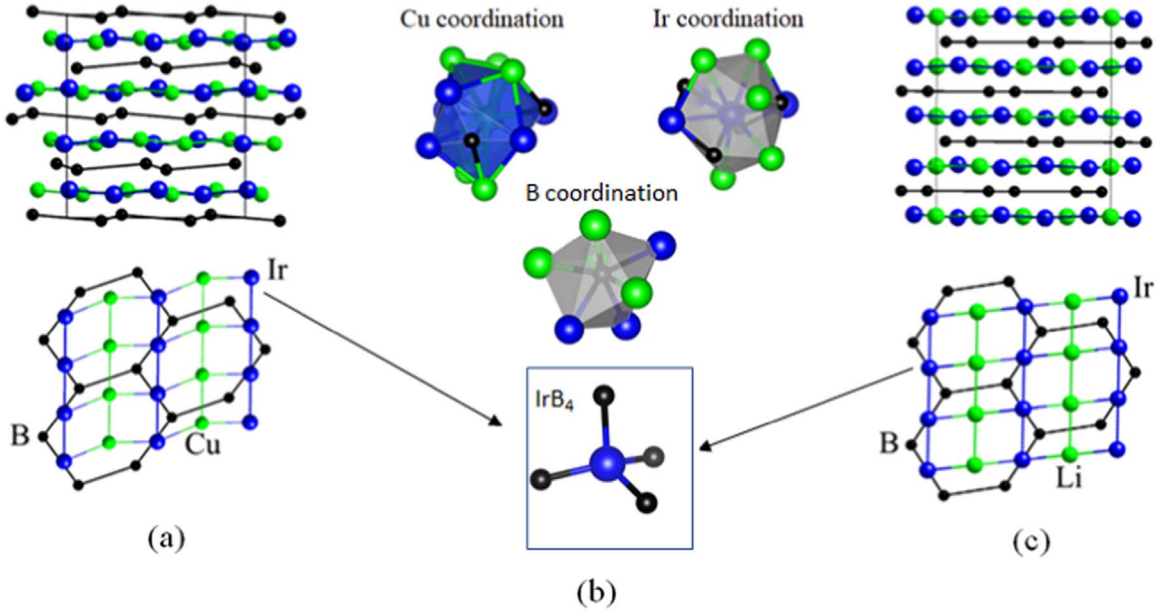

Fig. 8. (a) Structure of CuIrB (top) and its projection (below). (b) Coordination polyhedra around boron, copper and iridium and the IrB_4 building block. (c) Structure of LiIrB (top) and its projection (below).

which is very close to 0.5. In that case a statistical distribution of the boron atoms on that position could also result in neighboring boron atoms but with a very short distance of 1.62 Å. Since the occupancy for B2 is close to 0.5 and that such short B–B contacts are rarely observed, the authors proposed a reasonable structural model involving alternating B-filled and empty Ir_6-prisms as shown in (Fig. 9c).

2.4. *The* anti-*$CaCl_2$-type*

The crystal structure of Pd_2B is the only boride (with M:B = 2:1) known in the *anti*-$CaCl_2$-type, which was first reported by Lundström et al. [64,65] Pd_2B crystallizes in space group *Pnmm*, Pearson symbol *oP*6. It can be described as an orthorhombically distorted hexagonal close-packing of palladium atoms, with boron atoms filling one half of the octahedral voids (see Fig. 10a). The 6 palladium atoms around boron form slightly distorted octahedra (see Fig. 10b). The palladium atoms themselves are surrounded by 3 boron atoms and 12 (2 + 4 + 4 +2) palladium atoms (see Fig. 10b). The Pd–Pd distances in Pd_2B spread from 2.83 up to 3.11 Å. The Pd–B contacts are rather short with *d*(B–Pd) = 2.10–2.12 Å indicating strong interactions. B–B contacts are not observed in this structure. However, the structure needs further investigation as the positions of the boron atoms were not determined accurately.

2.5. *Pt_2B: One or two modifications?*

Sologub et al. reported in 2015 on a new structure type for Pt_2B crystallizing in the monoclinic space group *C*2/*m* (Pearson symbol: mC24). Fig. 11 shows how the structure can be interpreted as an intergrowth of two different structures; Pd_2B (anti-$CaCl_2$-type, Fig. 11) and CrB (TlI-type, Fig. 11). Pt_2B contains three Pt and two boron sites. The Pt2 site (green color in Fig. 11) is the only site susceptible to substitution as observed in $(Pt_{1-x}Cu_x)_2B$. The Pt atoms form a trigonal prism with rectangular faces joined around the boron atoms. These rectangular faces are similar to those observed in the CrB-type structure but unlike in the CrB structure there is no B-B zig-zag chains. Consequently, two types of metal coordinations are inherent for boron atoms: an octahedron and a trigonal prism. Pt_2B forms peritectically at 900 °C by the $L + Pt_3B_2 \leftrightarrow Pt_2B$ reaction and exists within a narrow concentration range [66].

Decades before the discovery of this new complex structure type for Pt_2B, another structure was reported (*anti*-MoS_2-type, space group: $P6_3/mmc$; Pearson symbol: *hP*6). This structure is shown in Fig. 12 and it contains $B[Pt_2]$ slabs stacked along the *c*-axis. The slab is formed by common edge sharing $B[Pt_6]$ trigonal prisms [64]. However, the Rietveld refinement of the X-ray powder diffraction data of the high-temperature phase of "Pt_3B" (applying the *anti*-MoS_2 structure model) did not provide satisfactory evidence for the assignment of this

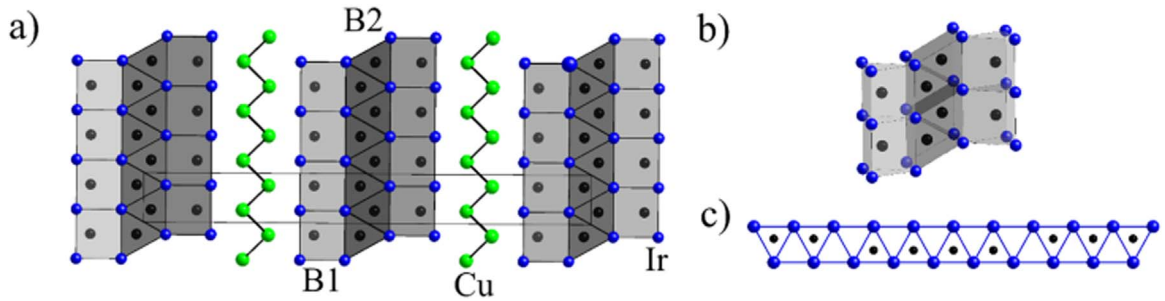

Fig. 9. The $Cu_2Ir_4B_3$-type: (a) Structure of $Cu_2Ir_4B_3$; (b) Ir/B sheet projected nearly along [100]; (c) Structural model for the disordered boron site (B2 site, 50% occupancy).

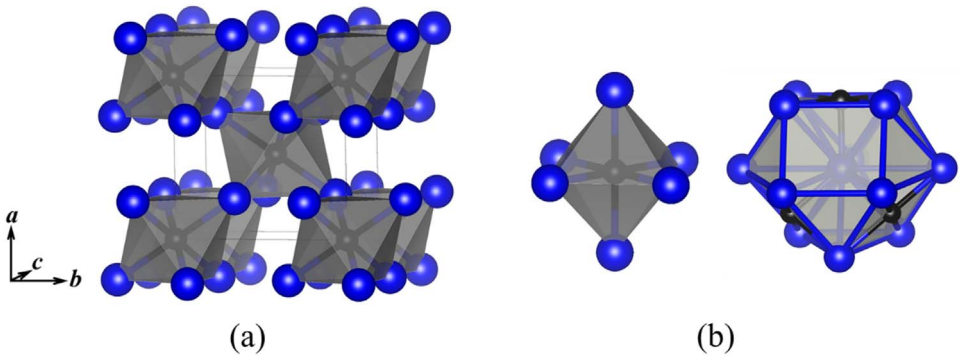

Fig. 10. The *anti*-$CaCl_2$-type, blue and black spheres represent Pd and B atoms, respectively. (a) Crystal structure of Pd_2B, projection nearly along [001]. (b) Coordination polyhedron around B and Pd. (For interpretation of the references to color in this figure, the reader is referred to the web version of this article).

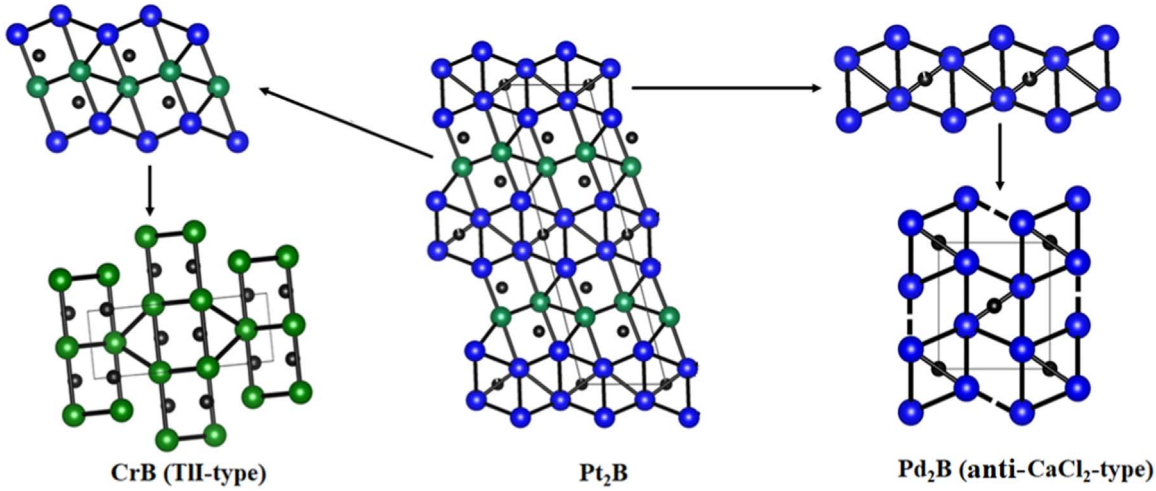

Fig. 11. (Middle) Crystal structure of Pt_2B (own type), an intergrowth of (left) CrB (TlI-type) and (right) Pd_2B (anti-$CaCl_2$-type). Color code: green (Pt2 or Cr), blue (Pt1 and Pt3 or Pd) and black (B). (For interpretation of the references to color in this figure legend, the reader is referred to the web version of this article).

structure type as reported by Sologub et al. [64], thus the *anti*-MoS_2-type structure for Pt_2B should be revised.

2.6. Co_2Si-type and its variants: Structural versatility enabled by multiple trigonal prisms connections

The Co_2Si-type (e.g. Rh_2B), TiNiSi-type (e.g. MoCoB), ZrNiAl-type (e.g. NbFeB) and NbCoB-type structures are all very closely related to each other (Table 4). Filled [M_6] trigonal prisms are the only building units of all these structures (Figs. 13a–16a). They connect with each other by sharing their triangular faces, thereby building rods that can be further connected through their edges. It is the type of edge connection of the rods that differentiates all these structures: For Co_2Si-type (e.g. Rh_2B) and its ternary variant TiNiSi-type (e.g. MoCoB) the edge connections of the rods lead to two identical 1D zigzag arrangements that are shifted by ½ from one another (Figs. 13a and 14a); for ZrNiAl- (e.g. NbFeB) and NbCoB-type, the edge connections lead to a 2D rod arrangement that enables the formation of large six-

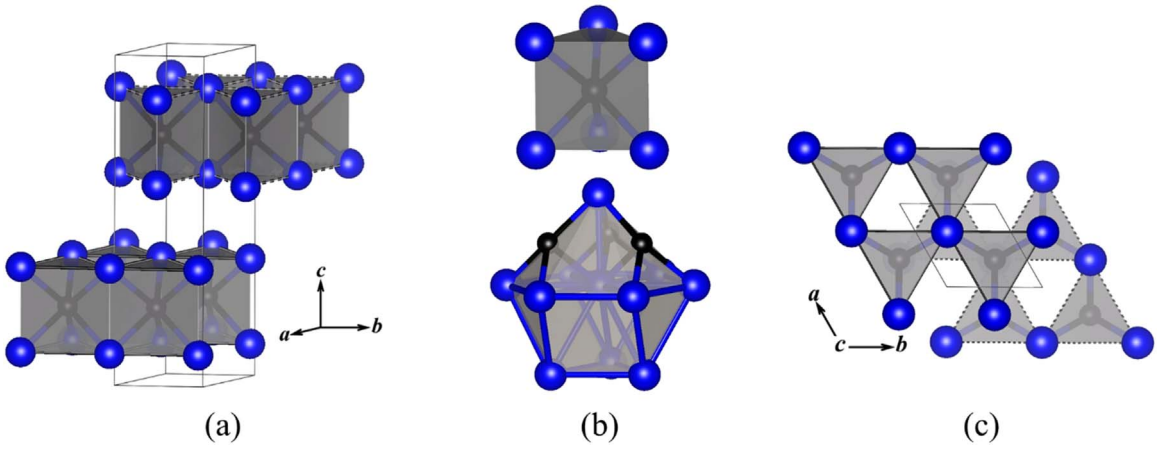

Fig. 12. The *anti*-MoS_2-type, blue and black spheres represent Pt and B atoms, respectively. (a) Crystal structure of Pt_2B; (b) Coordination polyhedron around B and Pt; b) Projection along [001], solid and dashed lines indicate two slabs.

Table 4
Compounds crystallizing in the Co_2Si-, TiNiSi-, ZrNiAl- and NbCoB-type structures.

Compound	Structure type	Space group	*a* (Å)	*b* (Å)	*c* (Å)	*V* (Å^3)	References
Rh_2B	Co_2Si	*Pnma*	5.42	3.98	7.44	160.5	[67]
WFeB	TiNiSi	*Pnma*	5.82	3.16	6.81	125.3	[98]
MoCoB	TiNiSi	*Pnma*	5.77	3.25	6.65	124.7	[98]
WCoB	TiNiSi	*Pnma*	5.75	3.20	6.65	122.4	[98]
ReCoB	TiNiSi	*Pnma*	5.65	3.22	6.55	119.2	[99]
NbFeB	ZrNiAl	$P\bar{6}2m$	6.02	6.02	3.22	101.1	[73]
TaFeB	ZrNiAl	$P\bar{6}2m$	5.98	5.98	3.20	99.1	[73]
NbCoB	NbCoB	*Pmmn*	3.27	17.18	5.95	334.3	[74]
TaCoB	NbCoB	*Pmmn*	3.26	17.07	5.92	329.4	[76]

membered ring channels which enclose an unconnected rod, the two of which are also displaced by ½ with respect to each other (Figs. 15a and 16a). The smallest lattice parameter of NbCoB, MoCoB (TiNiSi-type) and NbFeB (ZrNiAl-type) are all very close to each other, because they correspond to the height of the trigonal [BM_6] prisms. In the following, the borides found for these structure types will be discussed in more details.

2.6.1. Borides with Co_2Si-type structure and its ternary ordered variant TiNiSi

Rh_2B is the only boride reported to crystallize with Co_2Si-type structure. It was first reported by Welch et al. in 1954 and crystallizes in space group *Pnma* (Pearson symbol *oP*12) [67]. Boron atoms are coordinated by nine rhodium atoms (6 + 3) in the shape of a distorted trigonal prism with three faces capped (see Fig. 13c). The B–Rh distances vary from 2.37 Å up to 2.81 Å. The boron atom inside the trigonal prism is considerably shifted away from the center.

The TiNiSi-type (Space group: *Pnma*, Pearson symbol: *oP*12) is an ordered variant of the Co_2Si-type where the two metal atoms are located on separate crystallographic sites. For borides, boron occupies the 2 Si-sites, see for example the unit cell of MoCoB (Fig. 14). Further isotypic ternary compounds, WCoB, WFeB and ReCoB [68–71] have been reported. Interestingly, all these compounds contain a magnetic 3D element (Fe, Co), however no magnetic properties have been reported. A thin layer of WCoB, deposited on a carbide-cobalt hard alloy, was reported to be a superhard material with microhardness value of 45 GPa at a load of 0.5 N [72].

2.6.2. Borides with ZrNiAl and NbCoB structure types

Another boride structure based on B[M_6] trigonal prisms, NbFeB, was discovered in 1967. In fact, Kuz'ma and coworkers investigated the ternary system Nb-Fe-B and found that NbFeB adopts the ZrNiAl-type structure (space group $P\bar{6}2m$, Pearson symbol *hP*9), where Nb substitutes Zr, Fe replaces Al and B substitutes Ni (see Fig. 15 a). Nb and Ta typically show very similar structural chemistry, thus TaFeB was reported a year later to crystallize with the same structure type [73,74].

Boron, on each of its two crystallographic sites, is coordinated by a total of 9 metal atoms (see Fig. 15b). The shortest boron metal contacts are B–Fe with *d*(B–Fe) = 2.23–2.27 Å. B–Nb contacts range from 2.40 to 2.44 Å. Rather short heteroatomic metal contacts are found with *d*(Fe–Nb) = 2.62–2.67 Å, their homoatomic counterparts are larger with *d*(Fe–Fe) = 2.67–3.22 Å and *d*(Nb–Nb) = 3.18–3.22 Å. Boron-boron bonds are not observed in this structure.

In 1971 Krypyakevych et al. published a ternary boride with the formula NbCoB [75]. Its crystal structure is a combination of the TiNiSi- and the ZrNiAl-type structures. TaCoB is also reported to be isotopic with NbCoB [76]. NbCoB crystallizes in an orthorhombic unit cell with space group *Pmmn*, Pearson symbol: *oP*30. The structure of NbCoB (Fig. 16a) is also based on trigonal prismatic B[M_6] units but it is more complex than the above ones. Boron occupies three different crystallographic sites which leads to three different tricapped B[M_6] prisms (see Fig. 16b): B[Nb_6] capped with three Co atoms, B[Co_6] capped with three Nb atoms and B[Nb_4Co_2] capped with two Co and one Nb atoms. The B[Nb_6] prism shares three common edges with one B[Nb_6] and two B[Nb_4Co_2], whereas the B[Nb_4Co_2] prisms are connected with two B[Nb_6] by sharing their Nb-edges. This leads to the above-mentioned six membered rings forming channels along *a*, which host the B[Co_6] prisms.

The NbCoB-type can also be viewed as an intergrowth of the TiNiSi- and the ZrNiAl-types. Krypyakevych et al. have illustrated nicely [75] how the NbCoB-type can be generated by using the TiNiSi- and the ZrNiAl-type (Fig. 17c): The structure of NbCoB is derived by using two mirror-reflected MoCoB cells (Fig. 17b) which are then connected by six additional atoms located in both the 'vertical' and 'horizontal' *m* plane as found in the TiNiSi structure (see Fig. 17a).

All the above structures (beside $ZrCo_3B_2$) are made up of isolated boron atoms, however, our group and others have discovered new structure types which contain additional B_n fragments.

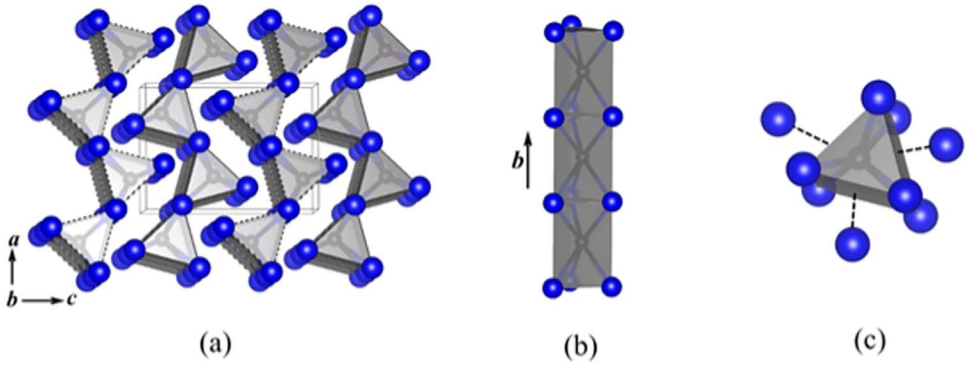

Fig. 13. The structure of Rh_2B ($CoSi_2$-type). (a) Projection nearly along [010] of the crystal structure of Rh_2B. (b) B[Rh_3] rod in Rh_2B. (c) B[Rh_6] trigonal prism with three rectangular faces capped by Rh. Dashed lines connect Rh atoms lying at y = ¼, solid lines connect Rh atoms lying at y = ¾. Blue and black spheres represent Rh and B atoms, respectively. (For interpretation of the references to color in this figure legend, the reader is referred to the web version of this article).

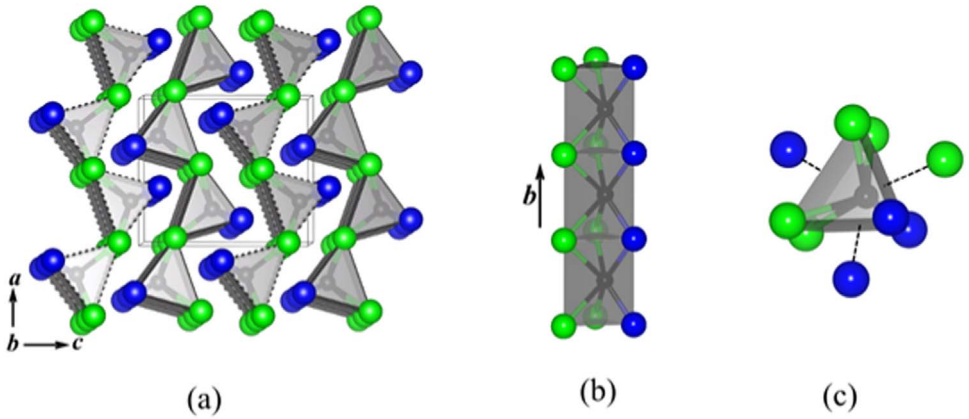

Fig. 14. The structure of MoCoB (TiNiSi-type), (a) Projection nearly along [010] of the crystal structure of MoCoB. (b) B[$(MoCo)_3$] rod in MoCoB. (c) B[$(MoCo)_6$] trigonal prism with three rectangular faces capped by Mo/Co. Solid lines connect metal atoms at y = ¼, dashed lines connect metal atoms at y = ¾. Blue, green and black spheres represent Co, Mo and B atoms, respectively. (For interpretation of the references to color in this figure legend, the reader is referred to the web version of this article).

3. Structures containing isolated boron atoms and B_n (n = 2-∞) units

3.1. Structures with isolated boron atoms and B_4 units

In 2006, our group reported on a new complex transition metal boride: $Ti_{1+x}Os_{2-x}RuB_2$ (x = 0.6), [21] The structure of which contains the firstly reported trigonal planar B_4 units, this was followed by the discovery of another complex quaternary boride, $Ti_{1+x}Rh_{2-x+y}Ir_{3-y}B_3$ (x = 0.68, y = 1.06) [22], in which zigzag B_4 units were found instead. $Ti_{1+x}Os_{2-x}RuB_2$ crystallizes in the hexagonal crystal system with space group $P\bar{6}2m$ (Pearson symbol *hP*18) while $Ti_{1+x}Rh_{2-x+y}Ir_{3-y}B_3$, which is closely related to the $Ti_{1+x}Os_{2-x}RuB_2$-type structure, crystallizes in the orthorhombic space group *Pbam* (Pearson symbol *oP*36).

3.1.1. $Ti_{1+x}Os_{2-x}RuB_2$-type containing isolated boron atoms and trigonal planar B_4 fragments

The crystal structure of $Ti_{1+x}Os_{2-x}RuB_2$ is shown in Fig. 18a, whereas Fig. 18b shows a view of the unit cell on the *bc*-plane [21]. The structure contains both isolated as well as connected B atoms which are located in the center of trigonal B[M_6] prisms (see Fig. 18a). The structure is built up by two layers which are alternating along the *c*-axis. One layer (*z* = ½) contains the M1 atoms (69% Os + 31% Ti) and the trigonal planar B_4 fragments (containing B1 and B2 atoms), and the other layer (*z* = 0) is filled with Ru atoms, M2 atoms (96% Ti + 4%Os) and isolated B atoms (B3). Although the two layers exhibit mixed atomic positions (M1 and M2) by Os and Ti, there is an obvious site-preferential tendency. The Os atoms mainly enter the layer at *z* = ½ whereas the Ti atoms are mostly found in the layer at *z* = 0. The prisms around B1 and B2 are found in groups of four but with a special trigonal arrangement (see Fig. 18a). There is one central B1[M_6] prism which shares its three rectangular faces with the prisms around the B2 atoms. Consequently, the distance between the B1 and B2 atoms is reduced, thereby leading to the formation of the trigonal planar B_4 units. The B-B distance in the B_4 fragment is *d*(B–B) = 1.89 Å so that it is expected to be a strong bond. Quantum chemical calculations with a subsequent COHP analysis confirmed very strong B–B bonding. The B2 –B1 –B2 angle measures 120° (see Fig. 18b). The isolated B3 atom, which is not located on the same layer as the B1 and B2 atoms, resides in a trigonal prism built up by six M1 atoms and capped by three M2 atoms (see Fig. 18c).

Table 5 lists all reported compounds in this structure type. Alongside the parent compound, variants like $Ti_{1.6}Os_{2.4}B_2$, $Ti_{1-x}Fe_xOs_2RhB_2$ (0 < x < 0.5) and $TiCrIr_2B_2$ have also been successfully synthesized [77,78]. In $TiCrIr_2B_2$ the presence of one-dimensional Cr_3 triangles was suggestive of possible magnetic frustration. Magnetic measurements showed ferrimagnetic-like behavior below 275 K with frustration parameter *f* = 2.7 [78]. VASP calculations indicate that the magnetic frustration originates from indirect antiferromagnetic Cr–Cr couplings within the Cr_3 triangles.

3.1.2. $Ti_{1+x}Rh_{2-x+y}Ir_{3-y}B_3$-type containing isolated boron atoms and zigzag B_4 fragments

The $Ti_{1+x}Rh_{2-x+y}Ir_{3-y}B_3$-type is closely related to the $Ti_{1+x}Os_{2-x}RuB_2$-type. The main difference between the two structures is the differing shape of the B_4 unit which has a zigzag shape in the $Ti_{1+x}Rh_{2-x+y}Ir_{3-y}B_3$-type [22]. Visualizing the structure along the [001] direction shows 2 different layers: the layer at *z* = ½ contains the trans B_4 zigzag fragments (B1, B2) and the mixed metal sites which have approximately the same Ir:Rh ratio (2:1). The other layer at *z* = 0

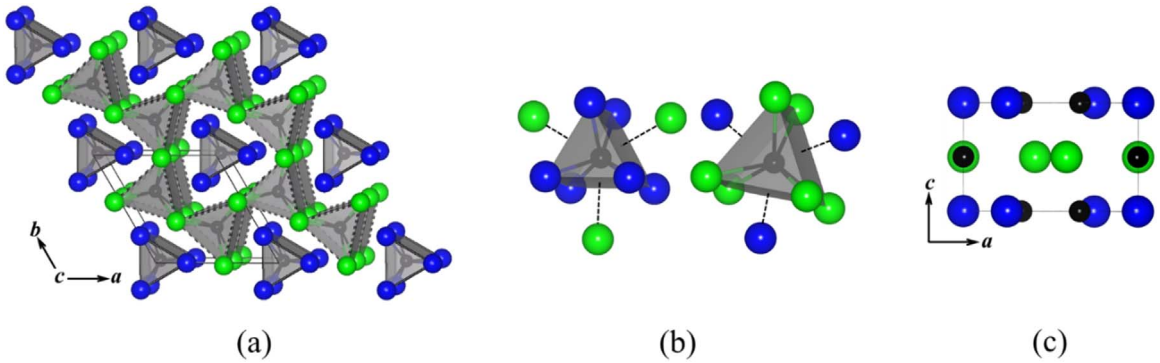

Fig. 15. (a) The structure of NbFeB (ZrNiAl-type), (b) Coordination polyhedra around boron. (c) View on the ac-plane. solid lines connect Fe atoms at z = 0, dashed lines connect Nb atoms at z = ½. Blue, green and black spheres represent Fe, Nb and B atoms, respectively. (For interpretation of the references to color in this figure legend, the reader is referred to the web version of this article).

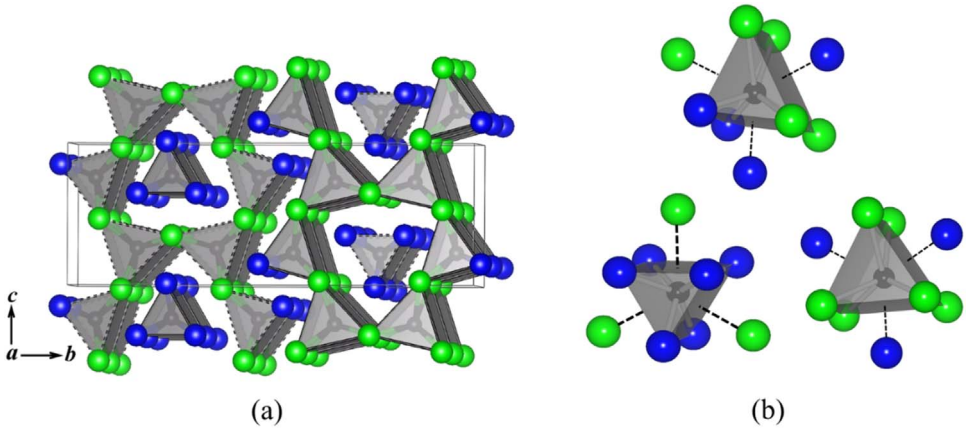

Fig. 16. (a) The crystal structure of NbCoB (own type), solid lines connect atoms lying at y = ¼, dashed lines connect atoms lying at y = ¾. Blue, green and black spheres represent Co, Nb and B atoms, respectively. b) Coordination polyhedra around boron. (For interpretation of the references to color in this figure legend, the reader is referred to the web version of this article).

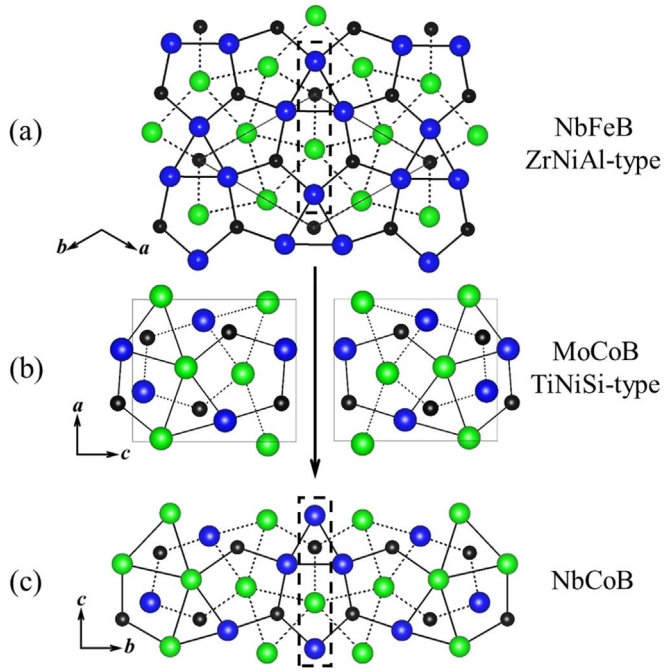

Fig. 17. Generation of the NbCoB-type out of a combination of the ZrNiAl-type and the TiNiSi-type. (a) NbFeB (ZrNiAl-type), view on the *ab*-plane, solid lines connect atoms with z = 0, dashed lines connect atoms with z = ½. (b) MoCoB (TiNiSi-type), view on the *ac*-plane (left) and ist mirrored image (right), solid lines connect atoms with z = ¼, dashed lines connect atoms with z = ¾. (c) View on the *bc*-plane of NbCoB.

contains isolated B (B3), Ti and Rh atoms, as well as the mixed metals with a Ti:Rh ratio of ca. 2:1. The boron atoms (B1, B2) which form the zigzag B_4 units reside in the $z = ½$ layer and at the center of trigonal B[M_6] prisms (Fig. 19a). These prisms are connected in groups by sharing common rectangular faces resulting in short B–B contacts. The B_4 unit has one central B1–B1 bond of 1.81 Å and two slightly larger B1–B2 bonds with a bond length of 1.87 Å (see Fig. 19b). The B1–B1–B2 angle measures ≈ 115° and the torsion angle of the four boron atoms is 180°, thus making this boron fragment planar. Similar zigzag-like B_4 fragments were found in the intermetallic borides Mo_2IrB_2 [79], α-Cr_2IrB_2 [59,80] and Ni_3ZnB_2 [59,80,81]. The B3 atoms enter the layer at $z = 0$ and are coordinated by a slightly distorted trigonal prisms capped by three Ti and mixed Ti/Rh atoms. The coordination environments for B-atoms are summarized in Fig. 19c.

While there is no group-subgroup relationship between the two $Ti_{1+x}Rh_{2-x+y}Ir_{3-y}B_3$- and $Ti_{1+x}Os_{2-x}RuB_2$-type structures, they contain similar 4*d*/5*d* transition metal framework as shown in Fig. 20. The 4*d*/5*d* transition metals form triangles which are linked with each other through metal-metal bonds to form six-membered rings. In the $Ti_{1+x}Os_{2-x}RuB_2$-type structure the six-membered rings have 3-fold rotational symmetry (see Fig. 20a), while the rings are distorted and no longer preserve the 3-fold rotational symmetry in the $Ti_{1+x}Rh_{2-x+y}Ir_{3-y}B_3$-type structure.

Recently Zheng et al. reported that TaRuB and NbOsB are ordered variants of the $Ti_{1+x}Rh_{2-x+y}Ir_{3-y}B_3$-type where alternating layers, along the [001] direction, have Ru (in TaRuB) or Os (in NbOsB) and the B_4 zigzag fragments in the z = ½ layer while in the z = 0 Ta (or Nb), and isolated B-atoms are found [82]. It must be added that both TaRuB and NbOsB also have two modifications (see section below and Table 6). The $Ti_{1+x}Rh_{2-x+y}Ir_{3-y}B_3$-type TaRuB reveals a bulk superconductivity at $T_C = 4$ K.

3.2. NbRuB-type structure with isolated boron atoms and B_2 units

NbRuB crystallizes in the orthorhombic space group *Pmma* (Pearson symbol *oP*16) [80]. The crystal structure is shown in Fig. 21a. NbRuB was synthesized by arc-melting the sample multiple times for 10 s. It was obtained as the majority phase (79%) with impurities of $Nb_3Ru_5B_2$ and NbB. Annealing the as-cast arc melted NbRuB below 1400 °C resulted in the formation of mainly $Nb_3Ru_5B_2$. The NbRuB structure is built up by two different structural features: The first is composed of isolated B atom coordinated by six Ru atoms to form B[Ru_6] trigonal prisms capped by three Nb atoms on the rectangular faces (see Fig. 21c). B[Ru_6] prisms stack along the *b* axis by sharing their triangular faces. The second feature is built up by B_2-dumbbells reside inside face-sharing double trigonal prisms, [B_2Nb_8] (see Fig. 21c). The double prisms share edges and form a zigzag chain along the *a*-axis. Rectangular faces in each prism of the double prisms is capped by two Ru atoms of the [Ru_6B] prisms and one B atom of the other prism. The B–B distance in the dumbbell is 1.88(3) Å. The structure shows four different metal sites, two Nb and two Ru sites. The two Ru atoms have strongly distorted icosahedral coordination by 12 atoms, Ru[$Nb_6Ru_3B_3$] and Ru[$Nb_6Ru_2B_4$] (Fig. 21c). The two Nb atoms are coordinated in pentagonal prisms Nb[Ru_6B_4] (Fig. 21c), showing just slight differences.

It was found that TaRuB also crystallizes in the NbRuB structure type along with the ordered variant of $Ti_{1+x}Rh_{2-x+y}Ir_{3-y}B_3$. Table 6 shows the synthetic conditions for obtaining the different structures of TaRuB. The NbRuB-type TaRuB is considered as the high temperature phase, as it was not observed until 1850 °C. The arc melted sample contained only 50% of TaRuB while the remaining product was made up of $Ta_3Ru_5B_2$ and TaB.

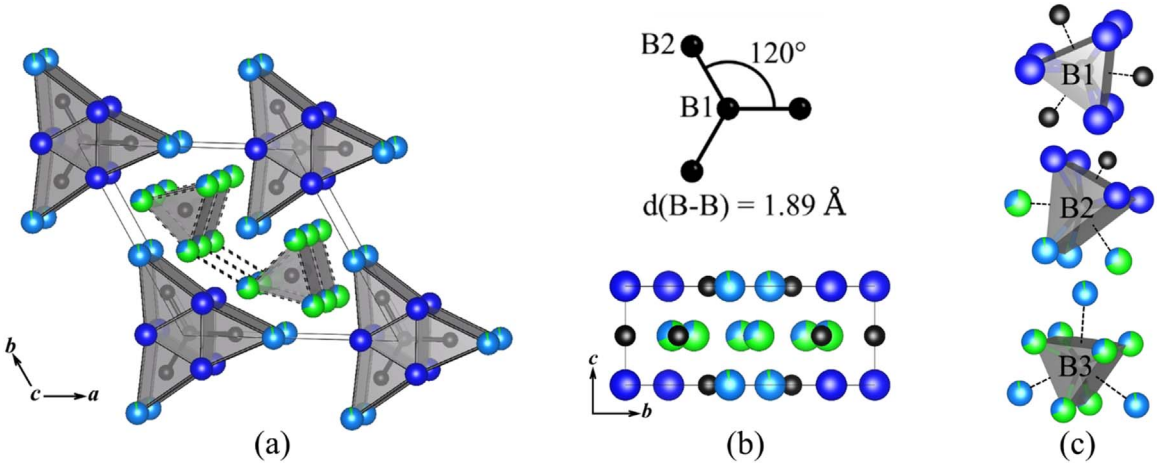

Fig. 18. (a) Crystal structure of $Ti_{1+x}Os_{2-x}RuB_2$ (own type). (b) A trigonal planar B_4 unit (top) and view on *bc*-plane (bottom). (c) Coordination polyhedra around B atoms. solid lines connect atoms at z = 0, dashed lines connect atoms at z = ½. Blue, light blue, green and black spheres represent Ru, Ti, Os and B atoms, respectively. (For interpretation of the references to color in this figure legend, the reader is referred to the web version of this article).

Table 5
Compounds crystallizing in the $Ti_{1+x}Os_{2-x}RuB_2$-type.

Compound	*a* (Å)	*c* (Å)	*V* (Å^3)	*References*
$Ti_{1.6}Os_{1.4}RuB_2$	8.83	3.03	204.7	[21]
$Ti_{1.6}Os_{2.4}B_2$	8.83	3.03	204.7	[77]
$(Ti_{0.75}Fe_{0.25})Os_2RhB_2$	8.83	3.03	204.6	[77]
$(Ti_{0.67}Fe_{0.33})Os_2RhB_2$	8.82	3.03	203.8	[77]
$TiCrIr_2B_2$	8.55	3.18	201.8	[78]

Fe, Ru and Os belong to the same group in the periodic table, yet they build different structures when combined with Nb and B. NbFeB builds the ZrNiAl-type structure while NbRuB has its own structure and NbOsB builds two structures (own type and $Ti_{1+x}Rh_{2-x+y}Ir_{3-y}B_3$-type). However, they all have strong structural similarities. The main similarity being that they are all built up from two types of trigonal prims that are shifted by ½ from one another in a given crystallographic direction: In NbFeB none of the prisms is face-connected through a rectangular face while in the Ru- and Os-phases the Nb-based prims are face-connected through a rectangular face. In fact, it is the type of face-connection that makes the difference between them, as it leads to the formation of different boron subunits: B_2 in NbRuB, trans zigzag B_4 in LT-NbOsB and zigzag B-chain in HT-NbOsB (see next section). It is possible to derive the crystal structure of NbRuB from that of NbFeB, by focusing on the Nb/B-framework. Starting with four interconnected B[Nb_6] prisms of the NbFeB structure (Fig. 22a) and reflecting the lower part of this unit as shown in Fig. 22b through a mirror plane, the Nb/B-framework as found in NbRuB will result (Fig. 22c).

NbRuB was found to be superconducting at 3.1 K. As reported by the authors, the sample contained impurities of $Nb_3Ru_5B_2$ and NbB, it was confirmed that pure samples of the impurity phases were not superconducting down to 0.4 K [83].

GGA-DFT calculations were performed to study the stability of TaRuB with the $Ti_{1+x}Rh_{2-x+y}Ir_{3-y}B_3$-type compared to the NbRuB-type. The results revealed that $Ti_{1+x}Rh_{2-x+y}Ir_{3-y}B_3$-type TaRuB is more stable by 3.98 kJ/mol [23].

3.3. HT-NbOsB-type structure with isolated boron atoms and infinite boron chains

The $Nb_{1+x}Os_{1-x}B$ structure crystallizes with its own structure type (Fig. 23) in the orthorhombic space group *Pnma* (Pearson symbol *oP*36) [24]. Like the above described structures, there are two main

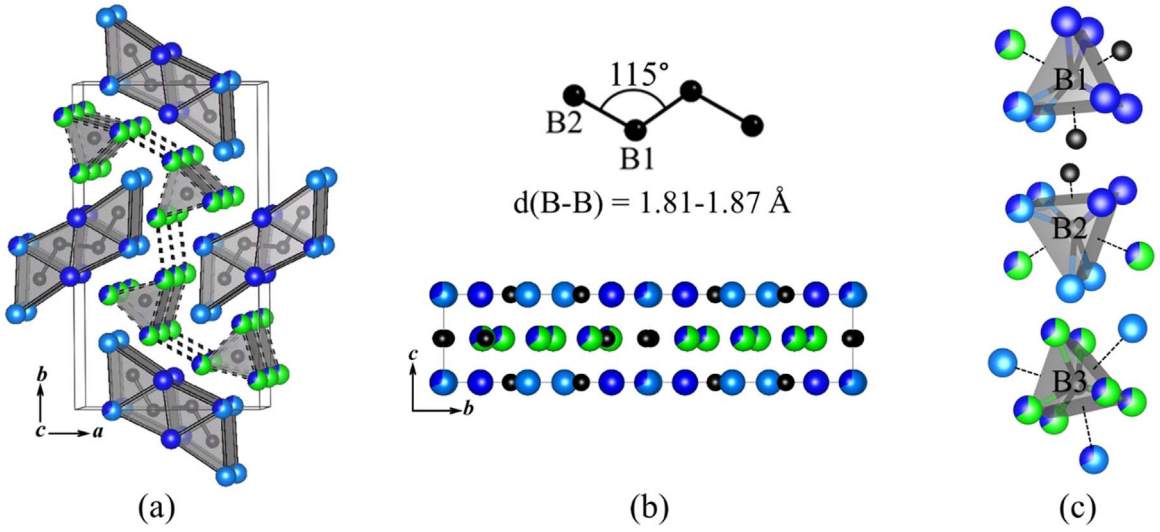

Fig. 19. (a) Crystal structure of $Ti_{1+x}Rh_{2-x+y}Ir_{3-y}B_3$ (own type). (b) Zigzag B_4 unit (top) and view on *bc*-plane (bottom). (c) Coordination polyhedra around B atoms. Solid lines connect atoms at z = 0, dashed lines connect atoms at z = ½. Blue, light blue, green and black spheres represent Rh, Ti, Ir and B atoms, respectively. (For interpretation of the references to color in this figure legend, the reader is referred to the web version of this article).

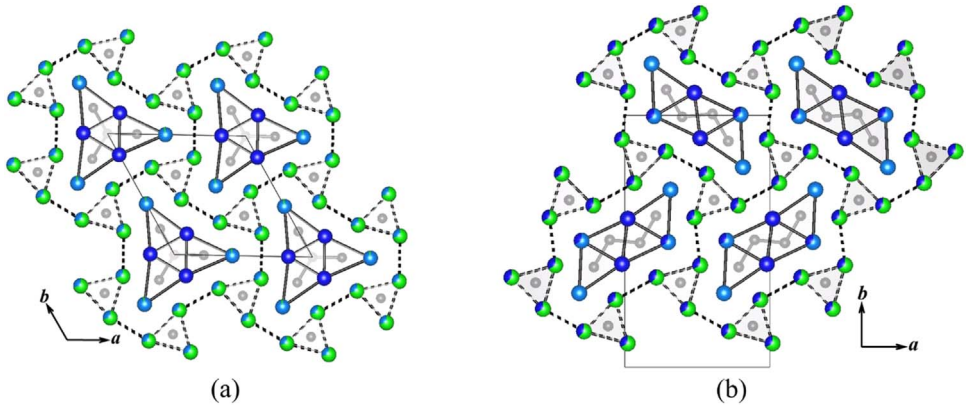

Fig. 20. Structural relationship between the $Ti_{1+x}Rh_{2-x+y}Ir_{3-y}B_3$- and the $Ti_{1+x}Os_{2-x}RuB_2$-type structures.

Table 6
Different modifications observed for TaRuB and NbOsB compositions and their synthesis.

Compound	Structure type	Space group	Boron fragments	Synthesis	Reference
TaRuB	$Ti_{1-x}Rh_{2+x-y}Ir_{3-y}B_3$	*Pbam*	B_4	Arc melting followed by annealing between 1500 and 1850 °C	[74]
	NbRuB	*Pmma*	B_2	Arc Melting	[75,76]
NbOsB	$Ti_{1-x}Rh_{2+x-y}Ir_{3-y}B_3$	*Pbam*	B_4	Arc melting followed by annealing between 1500 and 1850 °C	[74]
	HT-NbOsB	*Pnma*	B zigzag chain	Starting ratio $NbOs_2B_2$ for arc melted	[24]

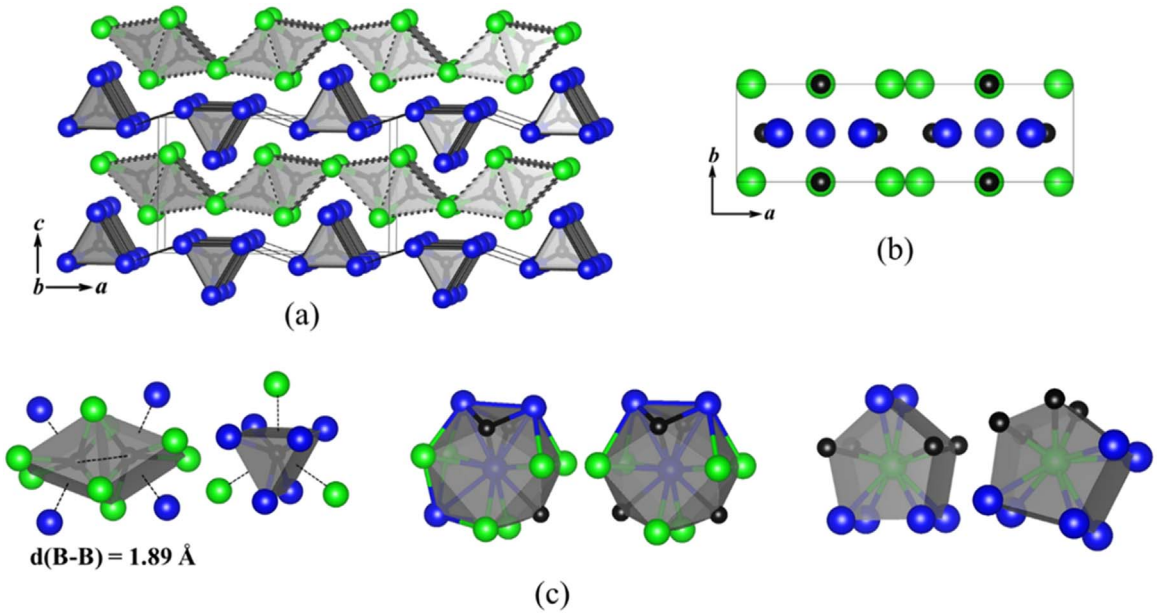

Fig. 21. The NbRuB-type. (a) Crystal structure of NbRuB. Solid lines connect atoms at z = 0, dashed lines connect atoms at z = ½. (b) View on the a*b*-plane. (c) Coordination polyhedron around B, Ru and Nb atom. Blue, green and black spheres represent Ru, Nb and B atoms, respectively. (For interpretation of the references to color in this figure legend, the reader is referred to the web version of this article).

building blocks for this structure based on the connectivity of the basic B-filled trigonal prims. The early transition metal (Nb) is responsible for the face-connected trigonal prisms while the late transition metal (Os) builds the isolated one. The main difference between this and the above-mentioned structures is that the face connection runs in 1D instead of building finite units. Consequently, infinite boron chains result and run perpendicular to the layer of the other trigonal prims which build edge-connected double prisms. The HT-NbOsB structure also has some similarities with the $Ni_{4-x}B_3$ structure type, as both contain isolated B-atoms as well as zigzag B-chains **(**Fig. 24**)**. An interesting difference between the NbRuB structure and the HT-$Nb_{1+x}Os_{1-x}B$ structure is the decrease in the bond length of the B–B from 1.88 Å to 1.77 Å. Similarly, there is a compression of the Nb–Nb bond length from 3.30 Å to 2.95 Å in the trigonal prisms. This compression in the structure maybe the reason for the partial substitution of Nb with Os in this structure to release the strain (see Fig. 25).

Table 6 shows the synthetic conditions for obtaining the different structures of NbOsB. HT-NbOsB can only be obtained when starting with a Nb:Os:B ratio of 1:2:2. DFT calculations suggested that the LT-NbOsB ($Ti_{1+x}Rh_{2-x+y}Ir_{3-y}B_3$-type) was the more stable structure (3.2 kJ/mol) but that HT-NbOsB was more stable than a hypothetical NbRuB-type NbOsB [24].

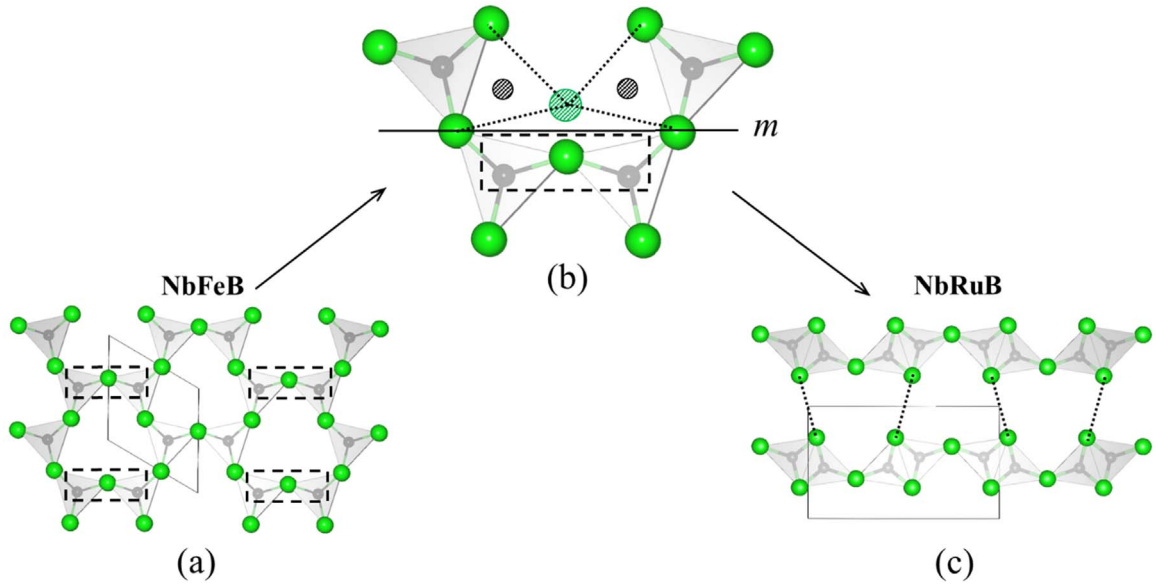

Fig. 22. Generation of the NbRuB-type out of NbFeB (ZrNiAl-type). Only the Nb framework of both structures are showed. (a) NbFeB view on the *ab*-plane. Dashed lines indicate the fragments concerned with the reflection as shown in (b), resulting in (c) NbRuB-type viewed on the *ac*-plane. Green and black spheres represent Nb and B atoms, respectively. (For interpretation of the references to color in this figure legend, the reader is referred to the web version of this article).

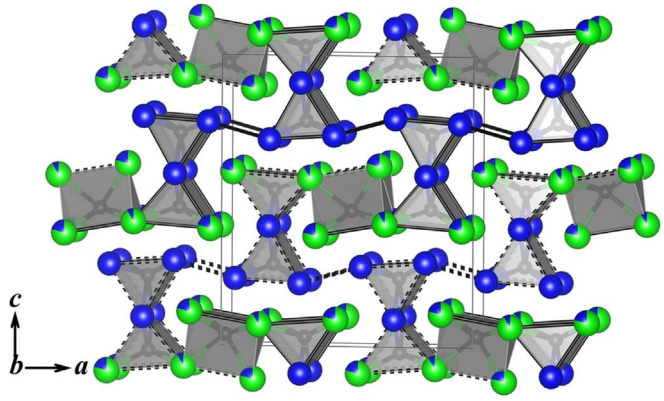

Fig. 23. Crystal structure of HT-NbOsB (own type). The prisms build completely by the green Nb-atoms share their rectangular faces in 1D thereby enabling the formation of zigzag B-chains along the b-axis perpendicular to the layer of double trigonal prisms. Solid lines connect atoms at z = 0, dashed lines connect atoms at z = ½. Blue, green and black spheres represent Os, Nb and B atoms, respectively. (For interpretation of the references to color in this figure legend, the reader is referred to the web version of this article).

4. Structures containing B_n (n = 4 - ∞) units and no isolated boron

This is a special group of structures with this M:B = 2:1 ratio because it is the only group without isolated boron atoms but with boron substructures instead. Beside the boron aggregation a metal aggregation in the form of metal layers is also found. Consequently, the boron-filled face-connected prims alternate in one direction with the metal layer, thereby creating layered structures. Table 7 summarizes the structures reported with zigzag B_n chains.

4.1. Ni_3ZnB_2-type containing zigzag B_4 fragments

Rogl et al. discovered a new structure type in the Ni-Zn-B system. The compound was refined with the chemical formula Ni_3ZnB_2 [81] and crystallizes in space group *C*2/*m* (Pearson symbol *mC*24). The Zn atoms form a puckered net of triangles and rectangles (see Fig. 26a). As can be seen in Fig. 26a, the structure of Ni_3ZnB_2 is built up by two different slabs and layers alternating along the *c*-axis. The Ni/B slab contains the B_4 fragments and the Zn sheet forms the puckered net.

The connection over rectangular faces of the B[Ni_6] prisms minimizes the distance between adjacent B atoms and consequently leads to zigzag like B_4-fragments with *d*(B–B) = 1.83–1.85 Å. The B–B–B angle measures ≈ 112° (see Fig. 26b). The boron-nickel contacts in Ni_3ZnB_2 with *d*(B–Ni) = 2.03–2.24 Å still indicate strong interactions, but as mentioned above, boron atoms are already involved in strong B–B bonding. B–Zn contacts *d*(B–Zn) = 2.42 Å are rather large and should play a subsidiary role only. Zn–Zn distances with *d*(Zn–Zn) = 2.59 –2.89 Å indicate metallic interactions inside the Zn-sheets. The tendency of Zn to form short homoatomic contacts resembles the typical behavior for a d^{10}-element as already observed for Cu in $Cu_2Ir_4B_3$ for example. Homoatomic nickel contacts *d*(Ni–Ni) = 2.54–2.99 Å are larger than in the element. Heteroatomic nickel-zinc contacts *d*(Ni–Zn) = 2.55–2.64 Å are of the same magnitude as the sum of their metallic radii.

4.2. MoAlB-type containing zigzag B-chain

In 1942, Halla and Thury first described MoAlB but reported the composition as $Mo_7Al_6B_8$ [84]. However in 1966, Jeitschko et al. refined the MoAlB structure (space *Cmcm*, Pearson symbol *oC*12) [85]. In 1995, Yu et al. presented the crystal growth from aluminium flux and the structure refinement of $Mo_{1-x}Cr_xAlB$ (x = 0,31) [86]. In 1968, NbNiB and TaNiB were also reported to crystallize in this structure type [87].

Recently, Hillebrecht et al. rationalized the relationship between the MoAlB (MAB) structure and the highly studied $M_{n+1}AX_n$ (MAX) phases (M = transition metals, A = group 13 and 14 elements, X = carbon and nitrogen and n = 1, 2 and 3) [88]. However, there are no reported MAX phases with X = B. MAX phases are layered structures, where the A-layer is sandwiched between the MX layers. These layered MAX phases are resistant to thermal shock and have high damage tolerence making them good ceramic materials [89].

Fig. 27a illustrates the structure of MoAlB which can be described as a layered structure with two sheets alternating along the *b*-axis. One sheet consists of B[Mo_6] prisms sharing two triangular and two rectangular faces in the *a* and *c*-directions, respectively. The other sheet is the aluminium bilayer in the *ac*-plane. Additionally, this structure contains infinite zig-zag boron chains (see Fig. 27b). It was also observed that the solid solutions of these MoAlB phases were possible with

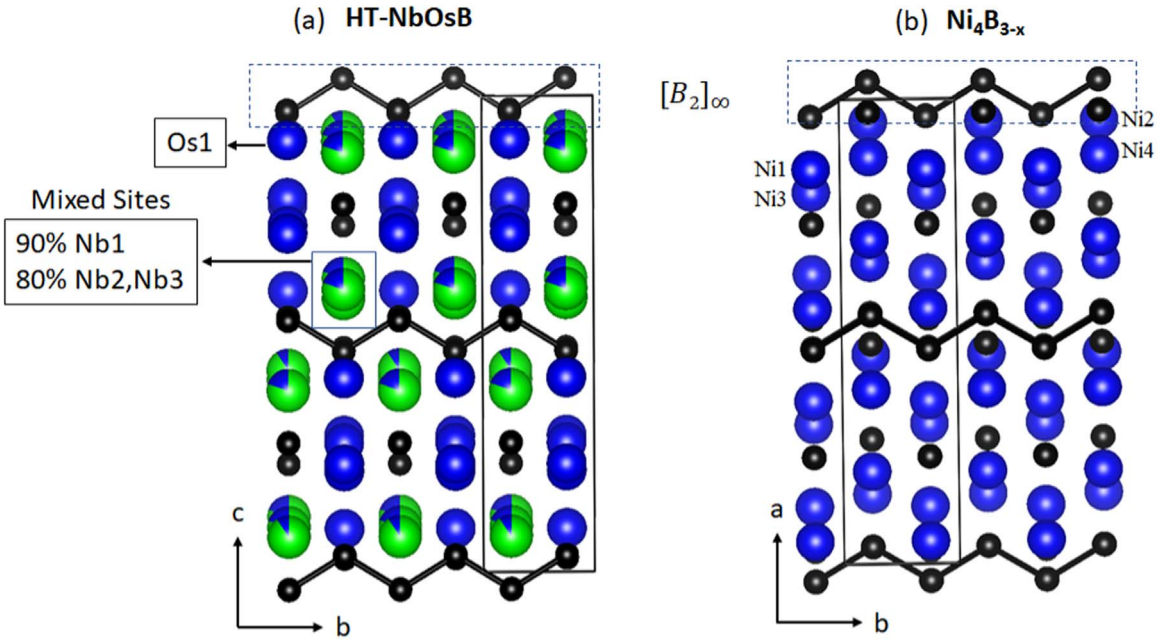

Fig. 24. Comparison between the HT-NbOsB and the Ni_4B_{3-x} structure, the infinite boron chains are highlighted.

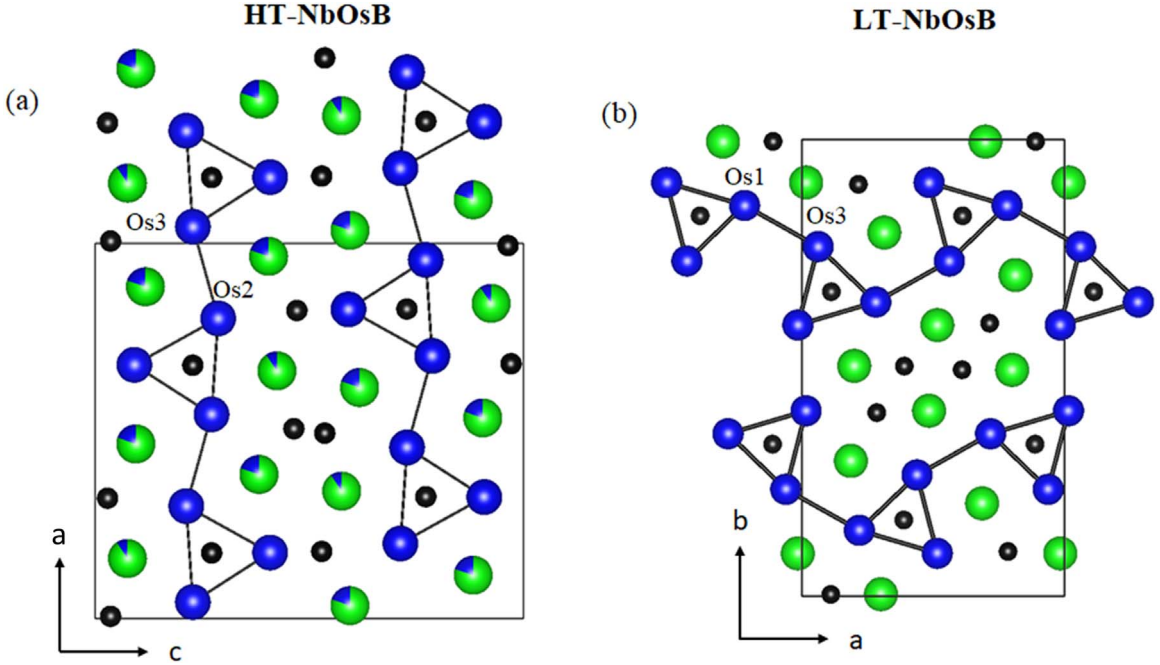

Fig. 25. (a) HT-NbOsB view on the *ac*-plane shows the alternating Os prisms. (b) the LT-NbOsB, in the $Ti_{1+x}Rh_{2-x+y}Ir_{3-y}B_3$ contains similar Os trigonal prisms but in a different arrangement. Green, blue and black spheres represent Nb, Os and B atoms, respectively.

Table 7
Compounds crystallizing in the MoAlB-type structures.

Compound	Structure type	Space group	Boron fragments
MoAlB	MoAlB	*Cmcm*	
WAlB	MoAlB	*Cmcm*	
$(W_{0.5}Mo_{0.5})AlB$	MoAlB	*Cmcm*	
$(Mo_{1-x}Cr_x)AlB$ x = 0.2, 0.39	MoAlB	*Cmcm*	B_∞ zigzag chain
NbNiB	MoAlB	*Cmcm*	
TaNiB	MoAlB	*Cmcm*	
Ni_3ZnB_2	Ni_3ZnB_2	*C2/m*	Zigzag B_4

substitution of the Mo site with Cr and W. MoAlB has shown good thermodynamic stability while WAlB shows relatively higher hardness and higher thermal conductivity [90]. Li et al. investigated the elastic, electronic and optical properties of MoAlB by first-principles calculation [91]. One of the problems observed in MAX phases as well as in the MAB phases is the formation of a passivating layer which reduces the possible applications of these materials [92]. There has been great interest in making these materials more robust and air stable.

Dimensional reduction of Ti_3AlC_2 by immersing it in hydrofluric acid resulted in the successful removal of the A layer (it is nearly impossibe to remove all Al) [93]. These 2D $M_{n+1}X_n$ layers were labelled as MAXenes (see Fig. 28a). Schaak et al. recently reported on the first microscopic evidence of an isolated MoB monolayer, demonstrating the

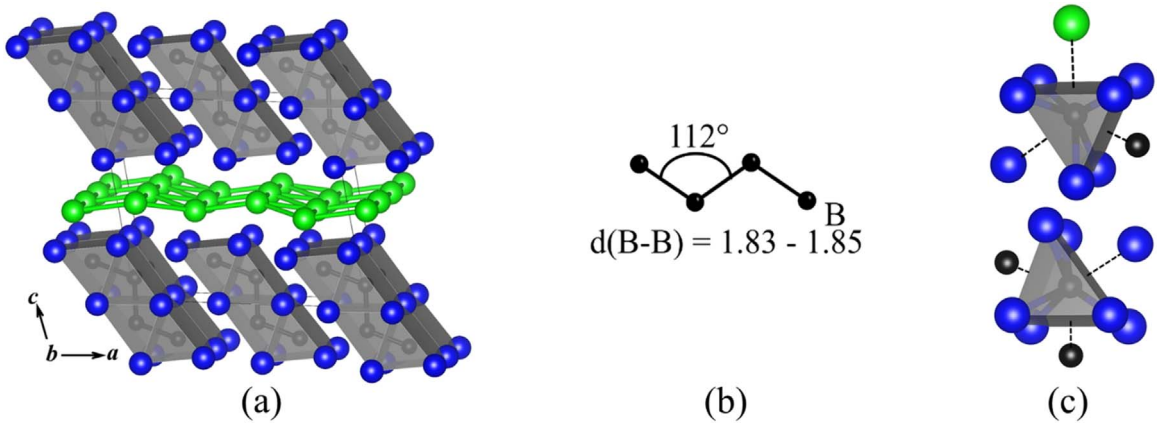

Fig. 26. (a) Crystal structure of Ni_3ZnB_2(own type). (b) Zigzag B_4 unit. (c) Coordination polyhedra around B atoms. Blue, green and black spheres represent Ni, Zn and B atoms, respectively.

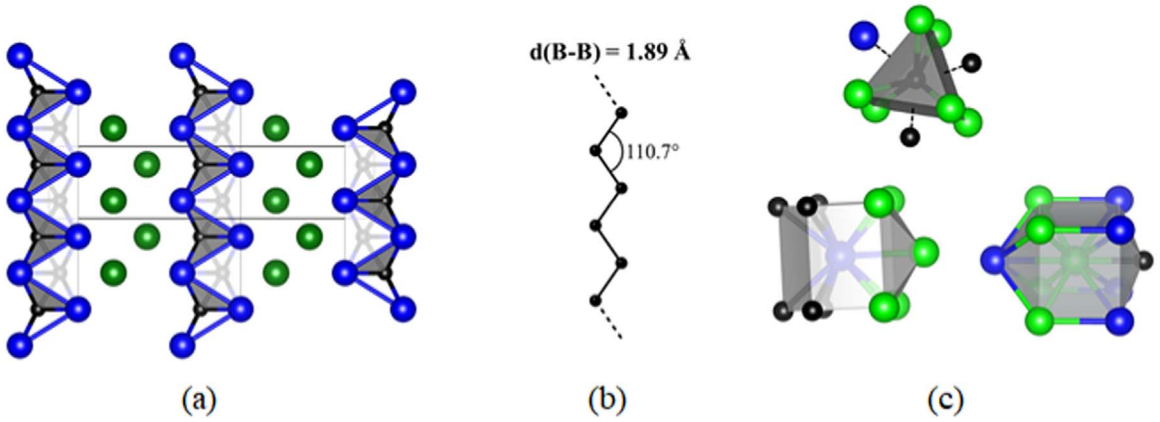

Fig. 27. (a) The Crystal structure of MoAlB (own type). (b) Zigzag boron chain. (c) Coordination polyhedra around B, Al and Mo atom. Blue, green and black spheres represent Mo, Al and B atoms, respectively.

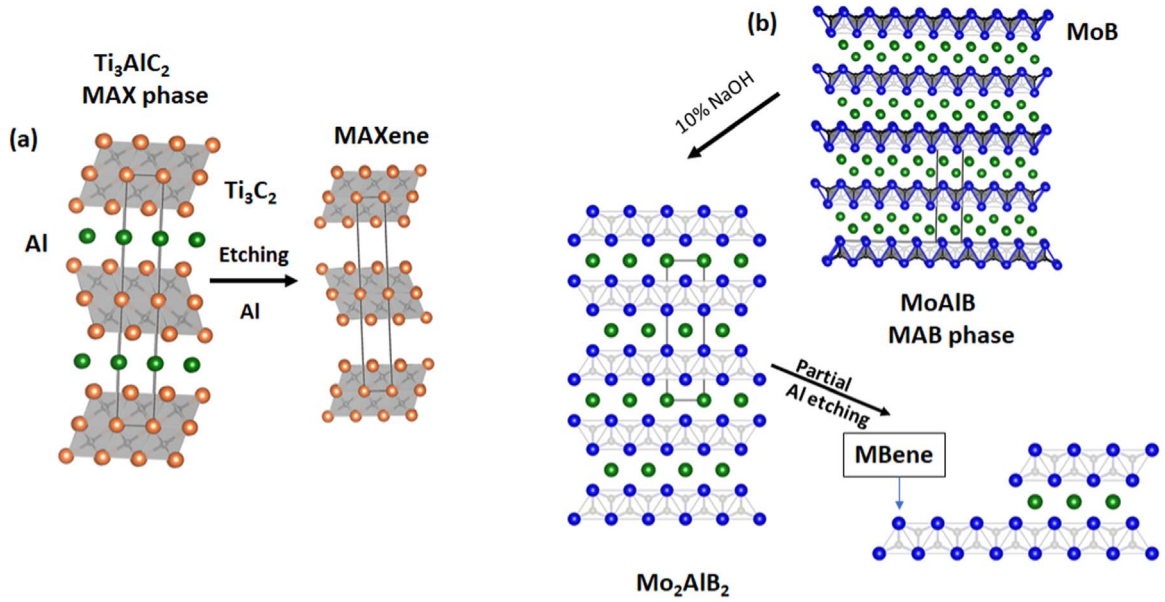

Fig. 28. Comparison between the MAX and the MAB crystal structures. (a) Etching of Al in Ti_3AlC_2 results in the MAXene phase made up of Ti_3C_2 layers (Al is difficult to remove completely). Orange, black and green spheres represent Ti, C and Al atoms, respectively. (b) MoAlB structure on top (MAB phase), partial etching pathways of Al to expose the MBene layers (MoB) via the formation of Mo_2AlB_2 (Cr_2AlB_2-type). Blue, black and green spheres correspond to Mo, B and Al atoms, respectively.

feasibility of using room-temperature metastable phase engineering and deintercalation (using NaOH) to access two-dimensional MBenes. The authors also observed that the deintercalation of Al lead to the formation of etched cavities resulting in a structure with a formula close to the hypothetical "Mo_2AlB_2" which is similar to the Cr_2AlB_2 structure as shown in Fig. 28b [94].

5. Conclusions

To the best of our knowledge the total number of structure types leading to intermetallic borides with a M: B-ratio of 2:1 is twenty-one. In nine of them (less than half) the occurrence of B–B-bonds (d(B–B) < 2.0 Å) is observed, indicating that most of these structures contain isolated boron atoms only. Several coordination environments for isolated boron atoms are found: The trigonal prismatic coordination (CN = 6(+3)), found in seventeen structure types, is by far the most important followed by the square anti-prismatic coordination (CN = 8). Two uncommon polyhedra around boron are found in the case of the CuIrB-type structure where an irregular coordination for boron with CN = 7 is found and in the *anti*-$CaCl_2$-type where an octahedral coordination around boron exist. Thus, the importance of the trigonal prismatic metal environment for boron atoms in metal-rich borides is evident in this review. Many structures of intermetallic borides are built up or contain such B[M_6] trigonal prisms and bonding analyses based on DFT calculations confirm strong bonding interactions for the B–M contacts so that they can be regarded as robust units. These prisms can be undistorted like in the $CeCo_3B_2$-type, where boron consequently resides in the exact center, but also distorted prisms are found like in the $CoSi_2$-type for example. Stronger distortions like in the $ZrCo_3B_2$-type can lead to the formation of short B–B-bonds (d(B–B) < 2.0 Å). Also, if the trigonal prisms share common rectangular faces, the capping metal atoms can be replaced by one or more boron atoms, leading to bonding between neighboring boron atoms. Due to the trigonal nature of the boron prisms the resulting fragments or chains are always angulated. Ni_3ZnB_2 and $Ti_{1+x}Rh_{2-x+y}Ir_{3-y}B_3$ are examples with zigzag B_4 fragments and in $Ti_{1+x}Os_{2-x}RuB_2$ trigonal planar B_4 fragments are found. In the case of the MoAlB-type the rectangular faces are shared in 1D leading to a zigzag chain.

Except for the anti-MoS_2-type (Pt_2B, existence is still debated), the trigonal prisms are stacked on top of each other and the direction of the stacking is parallel to the shortest crystallographic axis of the unit cell. Therefore, the short axis in these compounds is always close to 3.0 Å, which corresponds to the height of a typical B[M_6] prism. In the case of URu_3B_2 and $ZrCo_3B_2$ the short axis is doubled respectively tripled due to their superstructure in comparison to the related $CeCo_3B_2$-type.

These 2:1 metal borides also provide a great platform for electronic, physical and catalytic properties research. Even though interesting magnetic and superconducting properties have been found in many phases (especially in the $CeCo_3B_2$-type) as well as some fascinating catalytic behaviors (such as in $CuAl_2$-type phases), more must be done in the future to capitalize on the structural diversity from this 2:1 composition space.

Acknowledgement

We are grateful to Christian Goerens (Umicore, Germany) for his help during the early stage of writing this review. We thank UC Riverside (startup fund to BPTF) and the National Science Foundation Career award to BPTF (no. DMR-1654780) for financial support.

References

[1] B. Albert, H. Hillebrecht, Boron: elementary challenge for experimenters and theoreticians, Angew. Chem. Int. Ed. 48 (46) (2009) 8640–8668.
[2] B.P.T. Fokwa, Transition-metal-rich borides - fascinating crystal structures and magnetic properties, Eur. J. Inorg. Chem. 20 (2010) 3075–3092.
[3] B.P.T. Fokwa, Borides: solid-state chemistry, in: R.A. Scott (Ed.)Encyclopedia of Inorganic and Bioinorganic Chemistry, John Wiley & Sons, Ltd., 2014.
[4] T. Mori, Boron-Based Materials, CRC Press, Taylor & Francis Group, New York, 2016.
[5] G. Akopov, M.T. Yeung, R.B. Kaner, Rediscovering the crystal chemistry of borides, Adv. Mater. 29 (21) (2017).
[6] J.P. Scheifers, Y. Zhang, B.P.T. Fokwa, Boron: enabling exciting metal-rich structures and magnetic properties, Acc. Chem. Res. 50 (9) (2017) 2317–2325.
[7] R. Kiessling, The borides of some transition elements, Acta Chem. Scand. 4 (2) (1950) 209–227.
[8] K.P. Villars, Cenzual, Pearson's Crystal Data - Crystal Structure Database for Inorganic Compounds, ASM International, Materials Park, Ohio, USA, 2017 (/18).
[9] B. Aronsson, M. Backman, S. Rundqvist, The crystal structure of Re_3B, Acta Chem. Scand. 14 (5) (1960) 1001–1005.
[10] B. Aronsson, E. Stenberg, J. Aselius, Borides of rhenium and the platinum metals - the crystal structure of Re7B3, ReB_3, Rh_7B_3, $RhB_{1.1}$, $IrB_{1.1}$ and PtB, Acta Chem. Scand. 14 (3) (1960) 733–741.
[11] F. Bertaut, P. Blum, Etude des borures de chrome, Cr. Hebd. Acad. Sci. 236 (10) (1953) 1055–1056.
[12] T. Bjurström, Röntgenanalyse der systeme eisen-bor, kobalt-bor und nickel-Bor, Ark. Kemi Mineral. Geol. 11A (5) (1933) 1–12.
[13] J. Nagamatsu, N. Nakagawa, T. Muranaka, Y. Zenitani, J. Akimitsu, Superconductivity at 39 K in magnesium diboride, Nature 410 (6824) (2001) 63–64.
[14] L. Pauling, S. Weinbaum, The structure of calcium boride, CaB_6, Z. Krist. 87 (1/2) (1934) 181–182.
[15] J. Wong, T. Tanaka, M. Rowen, F. Schafers, B.R. Muller, Z.U. Rek, YB_{66} - a new soft X-ray monochromator for synchrotron radiation. II. Characterization, J. Synchrotron Radiat. 6 (1999) 1086–1095.
[16] J.F. Herbst, J.J. Croat, F.E. Pinkerton, W.B. Yelon, Relationships between crystal-structure and magnetic-properties in $Nd_2Fe_{14}B$, Phys. Rev. B 29 (7) (1984) 4176–4178.
[17] M. Sagawa, S. Fujimura, N. Togawa, H. Yamamoto, Y. Matsuura, New material for permanent-magnets on a base of Nd and Fe, J. Appl. Phys. 55 (6) (1984) 2083–2087.
[18] Y.B. Kuz'ma, Crystallochemistry of Borides, Lviv University Publishers, Lviv, 1983.
[19] B.Ba.J.-F. Halet, Chapter 5: Boron in Solid State Chemistry: Some Portraits of Metal Borides Taken from a Rich Structural Gallery, World Science Publishers, 2018.
[20] H. Park, A. Encinas, J.P. Scheifers, Y. Zhang, B.P.T. Fokwa, Boron-Dependency of Molybdenum Boride Electrocatalysts for the Hydrogen Evolution Reaction, Angew. Chem. Int. Ed. 56 (20) (2017) 5575–5578.
[21] B.P.T. Fokwa, J. von Appen, R. Dronskowski, Synthesis of a missing structural link: the first trigonal planar B-4 units in the novel complex boride Ti1+xOs2-xRuB2 (x=0.6), Chem. Commun. 42 (2006) 4419–4421.
[22] C. Goerens, B.P.T. Fokwa, The complex metal-rich boride $Ti_{1+x}Rh_{2-x+y}Ir_{3-y}B_3$ (x=0.68, y=1.06) with a new structure type containing B-4 zigzag fragments: synthesis, crystal chemistry and theoretical calculations, J. Solid State Chem. 192 (2012) 113–119.
[23] M. Mbarki, R. St Touzani, C.W.G. Rehorn, F.C. Gladisch, B.P.T. Fokwa, New ternary tantalum borides containing boron dumbbells: experimental and theoretical studies of Ta_2OsB_2 and TaRuB, J. Solid State Chem. 242 (2016) 28–33.
[24] R. Forsythe, J.P. Scheifers, Y. Zhang, B.P.T. Fokwa, HT-NbOsB: experimental and theoretical investigations of a boride structure type containing boron chains and isolated boron atoms, Eur. J. Inorg. Chem. 28 (2018) 3297–3303.
[25] Y.B. Kuz'ma, P.I. Krypyakevich, N.S. Bilonishko, Crystal structure of $CeCo_3B_2$ and analogous compounds, Dopov. Akad. Nauk Ukr. RSR, Ser. A (1969) 939–941.
[26] H.C. Ku, G.P. Meisner, Crystal-structure and physical-properties of new ternary rare-earth borides, J. Less-Common Met. 78 (1) (1981) 99–107.
[27] M. Vlasse, T. Ohtani, B. Chevalier, J. Etourneau, The crystal-structure of a new magnetic ternary boride $Nd_{0.71}Rh_{3.29}B_2$, J. Solid State Chem. 46 (2) (1983) 188–192.
[28] P. Rogl, The crystal-structure of URu_3B_2, J. Nucl. Mater. 92 (2–3) (1980) 292–298.
[29] Y.V. Voroshilov, P.I. Kripyake, Y.B. Ku'zma, Crystal structures of $ZrCo_3B_2$ and $HfCo_3B_2$, Sov. Phys. Crystallogr. 15 (5) (1971) 813–816.
[30] P. Rogl, Rare earth-cobalt borides, Mon. Chem. 104 (6) (1973) 1623–1631.
[31] K. Niihara, S. Yajima, Preparation and crystal-structure of ternary rare-earth borides, $RECo_3B_2$, B. Chem. Soc. Jpn. 46 (3) (1973) 770–774.
[32] H.C. Ku, G.P. Meisner, F. Acker, D.C. Johnston, Superconducting and magnetic-properties of new ternary borides with the $CeCo_3B_2$-type structure, Solid State Commun. 35 (2) (1980) 91–96.
[33] O. Sologub, C. Rizzoli, P. Salamakha, H. Ipser, Structural investigation of ternary $REIr_3B_2$ compounds (RE=Ce and Pr), J. Alloy Compd. 360 (1–2) (2003) 127–130.
[34] I.P. Valovka, Y.B. Kuzma, New ternary borides with structures of $CeCo_3B_2$ and $CeCo_4B$ type, Dopov. Akad. Nauk. A 11 (1974) 1029–1031.
[35] M. Dias, P.A. Carvalho, L.C.J. Pereira, I.C. Santos, O. Tougait, V.H. Tran, A.P. Goncalves, Crystal structure and magnetism of UFe_3B_2, J. Magn. Magn. Mater. 324 (17) (2012) 2649–2653.
[36] H.N. Nowotny, Die Kristallstrukturen von Ni_5Ce, Ni_5La, Ni_5Ca, Cu_5La, Cu_5Ca, Zn_5La, Zn_5Ca, Ni_2Ce, MgCe, MgLa und MgSr, Z. Metallkd. 34 (1942) 247–253.
[37] T. Shishido, J.H. Ye, M. Oku, S. Okada, K. Kudou, T. Sasaki, T. Matsumoto, T. Fukuda, Crystal growth and characterizations of $ErRh_3B_2$, J. Alloy Compd. 248 (1–2) (1997) 18–23.
[38] K. Kubota, E. Matsuoka, Y. Funasako, T. Mochida, T. Sakurai, H. Ohta, T. Onimaru, T. Takabatake, H. Sugawara, Weak Ferromagnetism below 41K and Structural Transition at 395K in $CeIr_3$B2 Single Crystal, J. Phys. Soc. Jpn. 82 (10) (2013).
[39] J.H. Ye, T. Shishido, T. Fukuda, K. Nakajima, Crystal growth and structural properties of $RERh_3B_2$ (RE = Gd, Er, Tm) compounds, J. Cryst. Growth 229 (1) (2001) 521–526.
[40] Y. Abe, M. Kasaya, I. Higashi, Y. Iimura, H. Yoshida, G. Kido, T. Kasuya, Magnetic and structural phase-transitions in $SmRh_3B_2$, J. Magn. Magn. Mater. 90–1 (1990) 567–568.
[41] H. Ido, M. Nanjo, M. Yamada, Magnetic-susceptibility of $RECo_3B_2$ (RE=Y, Sm, Gd, and Dy), J. Appl. Phys. 75 (10) (1994) 7140–7142.

[42] L.W. Li, K. Nishimura, H. Igawa, D.X. Huo, Magnetic properties and magnetocaloric effect in $GdCo_3B_2$ compound, J. Alloy Compd. 509 (11) (2011) 4198–4200.
[43] M. Dubman, E.N. Caspi, H. Ettedgui, L. Keller, M. Melamud, H. Shaked, Magnetic ordering and spin-reorientation transitions in TbCo3B2, Phys. Rev. B 72 (2) (2005).
[44] L.W. Li, D.X. Huo, H. Igawa, K. Nishimura, Large magnetocaloric effect in $TbCo_3B_2$ compound, J. Alloy Compd. 509 (5) (2011) 1796–1799.
[45] X.Q. Zheng, J.W. Xu, H. Zhang, J.Y. Zhang, S.G. Wang, Y. Zhang, Z.Y. Xu, L.C. Wang, B.G. Shen, Magnetic properties and magnetocaloric effect of $HoCo_3B_2$ compound, AIP Adv. 8 (5) (2018).
[46] L.W. Li, K. Nishimura, D.X. Huo, Z.H. Qian, T. Namiki, Critical behaviour of the RCo_3B_2 (R = Gd, Tb and Dy) compounds, J. Alloy Compd. 572 (2013) 205–208.
[47] P. Eckerlin, H. Kandler, Structure Data of Elements and Intermetallic Phases · 1966 - 1969: Datasheet from Landolt-Börnstein - Group III Condensed Matter, in: K.H. Hellwege, A.M. Hellwege (Eds.), Structure Data of Elements and Intermetallic Phases, Springer-Verlag, Berlin, Heidelberg, 1971 https://dx.doi.org/10.1007/10201454_74.
[48] E.E. Havinga, P. Hokkeling, H. Damsma, Compounds and pseudo-binary alloys with $CuAl_2$ (C16)-type structure .1. preparation and X-Ray results, J. Less-Common Met. 27 (2) (1972) 169–186.
[49] E.E. Havinga, Compounds and pseudo-binary alloys with $CuAl_2$ (C16)-type structure ii. theoretical discussion of crystallographic parameters, J. Less-Common Met. 27 (2) (1972) 187.
[50] E.E. Havinga, H. Damsma, Compounds and pseudo-binary alloys with $CuAl_2$(C16)-type structure III. stability and competitive structures, J. Less-Common Met. 27 (3) (1972) 269–280.
[51] E.E. Havinga, H. Damsma, J.M. Kanis, Compounds and pseudo-binary alloys with $CuAl_2$ (C16)-type structure .4. Superconductivity, J. Less-Common Met. 27 (3) (1972) 281–291.
[52] M.D. Kuz'min, K.P. Skokov, H. Jian, I. Radulov, O. Gutfleisch, Towards high-performance permanent magnets without rare earths, J. Phys.-Condens. Matter 26 (6) (2014).
[53] A. Edstrom, M. Werwinski, D. Iusan, J. Rusz, O. Eriksson, K.P. Skokov, I.A. Radulov, S. Ener, M.D. Kuz'min, J. Hong, M. Fries, D.Y. Karpenkov, O. Gutfleisch, P. Toson, J. Fidler, Magnetic properties of $(Fe_{1-x}Co_x)_2B$ alloys and the effect of doping by 5d elements, Phys. Rev. B 92 (17) (2015).
[54] N. Kalyon, K. Hofmann, J. Malter, M. Lucas, P. Claus, B. Albert, Catalytic activity of nanoscale borides: Co_2B and Ni_7B_3 in the liquid-phase hydrogenation of citral, J. Catal. 352 (2017) 436–441.
[55] S. Klemenz, J. Schuch, S. Hawel, A.M. Zieschang, B. Kaiser, W. Jaegermann, B. Albert, Synthesis of a highly efficient oxygen-evolution electrocatalyst by incorporation of iron into nanoscale cobalt borides, ChemSusChem 11 (2018) 1–8.
[56] J. Masa, P. Weide, D. Peeters, I. Sinev, W. Xia, Z.Y. Sun, C. Somsen, M. Muhler, W. Schuhmann, Amorphous cobalt boride (Co_2B) as a highly efficient nonprecious catalyst for electrochemical water splitting: oxygen and Hydrogen Evolution, Adv. Energy Mater. 6 (12) (2016) 1502313.
[57] M. O'Keeffe, S. Andersson, Rod packings and crystal-chemistry, Acta Crystallogr. A 33 (6) (1977) 914–923.
[58] J.L. Andrieux, S. Marion, Sur la preparation electrolytique des borures de chrome, Cr. Hebd. Acad. Sci. 236 (8) (1953) 805–807.
[59] D. Kotzott, M. Ade, H. Hillebrecht, Synthesis and crystal structures of alpha- and beta-modifications of Cr_2IrB_2 containing 4-membered B-4 chain fragments, the tau-boride $Cr_{7.9}Ir_{14.1}B_6$ and orthorhombic Cr_2B, Solid State Sci. 10 (3) (2008) 291–302.
[60] C.N. Guy, A.A. Uraz, Chromium-boron system, J. Less-Common Met. 48 (2) (1976) 199–203.
[61] L.E. Tergenius, Refinement of the crystal-structure of orthorhombic Mn_2B (formerly denoted Mn_4B), J. Less-Common Met. 82 (1981) 335–340.
[62] W. Klunter, B. Schmidt, W. Jung, LiIrB, CuIrB and PdIrB, ternary iridium borides with new $CaRh_2B_2$-type structures, J. Alloy Compd. 205 (1–2) (1994) 93–100.
[63] W. Klunter, W. Jung, The copper iridium boride $Cu_2Ir_4B_3$ with a layer structure derived from the $ZnIr_4B_3$ type, Z. Anorg. Allg. Chem. 626 (2) (2000) 502–505.
[64] E. Hassler, T. Lundstrom, L.E. Tergenius, Crystal-chemistry of platinum metal borides, J. Less-Common Met. 67 (2) (1979) 567–572.
[65] L.E. Tergenius, T. Lundstrom, Crystal-structure of Pd2b, J. Solid State Chem. 31 (3) (1980) 361–367.
[66] O. Sologub, L. Salamakha, P. Rogl, B. Stoger, E. Bauer, J. Bernardi, G. Giester, M. Waas, R. Svagera, Pt-B system revisited: Pt_2B, a new structure type of binary borides. ternary WAI_{12}-type derivative borides, Inorg. Chem. 54 (22) (2015) 10958–10965.
[67] R.W. Mooney, A.J.E. Welch, The crystal structure of Rh_2B, Acta Crystallogr. B 7 (1) (1954) 49–53.
[68] H. Haschke, H. Nowotny, F. Benesovs, Investigations of 3-component systems (Mo W)-(Fe Co Ni)-B, Mon. Chem. 97 (5) (1966) 1459 (- &).
[69] H.H. Stadelmaier, H.H. Davis, Cobalt region in 3-component system cobalt-molybdenum-boron, Mon. Chem. 97 (5) (1966) 1489.
[70] W. Jeitschko, The crystal structure of MoCoB and related compounds, Acta Crystallogr. B 24 (1967) 930–934.
[71] M.V. Chyepiga, Y.B. Kuz'ma, P.I. Krypyakevych, Crystal structure of compounds in the Chromium-nickel-boron and rhenium-cobalt-boron systems, Tezizy Dokl. Vses. Konf. Krist. Intermet. Soeden. 1 (1971) 33.
[72] Z.T. Zahariev, M.I. Marinov, Superhard boride layer deposition on a carbide cobalt hard alloy, J. Alloy Compd. 201 (1993) 1–3.
[73] Y.B. Kuz'ma, Crystal structures of NbFeB and TaFeB compounds, Dopov. Akad. Nauk Ukr. RSR, Ser. A (1967) 939–940.
[74] Y.B. Kuz'ma, T.I. Tsolkovskii, O.P. Baburova, The systems niobium-iron-boron and niobium-cobalt-boron, Inorg. Mater. 4 (1968) 950–953.
[75] P.I. Krypyakevich, Y.B. Kuz'ma, Y.V. Voroshilov, C.B. Shoemaker, D.P. Shoemaker, Crystal structure of NbCoB, Acta Cryst. B-Stru. B 27 (Feb15) (1971) 257–261.
[76] Y.B. Kuz'ma, O.M. Rudakevich, Crystalline-structure of compounds TaCoB and $NbCoB_2$, Dopov. Akad. Nauk A 2 (1973) 164–167.
[77] B.P.T. Fokwa, R. Dronskowski, New transition-metal borides containing trigonal-planar B(4)-units: syntheses and single-crystal structure analyses of Ti(1.6)Os(2.4)B(2) and Ti(1-x)Fe(x)Os(2)RhB(2) ($0 < x < 0.5$), Z. Anorg. Allg. Chem. 634 (11) (2008) 1955–1960.
[78] M. Kupers, L. Lutz-Kappelman, Y. Zhang, G.J. Miller, B.P.T. Fokwa, Spin frustration and magnetic ordering from one-dimensional stacking of Cr-3 triangles in $TiCrIr_2B_2$, Inorg. Chem. 55 (11) (2016) 5640–5648.
[79] P. Rogl, F. Benesovs, H. Nowotny, Complex borides with platinum metals, Mon. Chem. 103 (4) (1972) 965.
[80] P. Rogl, H. Nowotny, New phases with Mo_2IrB_2-type, Rev. Chim. Miner. 11 (5) (1974) 547–555.
[81] Z.P. Malik, O. Sologub, A. Grytsiv, G. Giester, P.F. Rogl, Crystal structure of novel Ni-Zn borides: first observation of a boron-metal nested cage unit: $B_{20}Ni_6$, Inorg. Chem. 50 (16) (2011) 7669–7675.
[82] Q. Zheng, R. Gumeniuk, H. Rosner, W. Schnelle, Y. Prots, U. Burkhardt, Y. Grin, A. Leithe-Jasper, Synthesis, crystal structure and properties of the new superconductors TaRuB and NbOsB, J. Phys. -Condens. Mat. 27 (41) (2015) 415701.
[83] W.W. Xie, H.X. Luo, K. Baroudi, J.W. Krizan, B.F. Phelan, R.J. Cava, Fragment-based design of NbRuB as a new metal-rich boride superconductor, Chem. Mater. 27 (4) (2015) 1149–1152.
[84] F. Halla, W. Thury, On borides of molybdenum and tungsten, Z. Anorg. Allg. Chem. 249 (3) (1942) 229–237.
[85] W. Jeitschko, Crystal structure of MoAlB, Mon. Chem. 97 (5) (1966) 1472–1476.
[86] Y. Yu, T. Lundstrom, Crystal-growth and structural investigation of the new quaternary compound $Mo_{1-x}Cr_xAlB$ with x=0.39, J. Alloy Compd. 226 (1–2) (1995) 5–9.
[87] Y.B. Kuz'ma, Crystalline structures of compounds NbNiB and TaNiB, Sov. Phys. Crystallogr. 13 (4) (1969) 597–598.
[88] M. Ade, H. Hillebrecht, Ternary borides Cr_2AlB_2, Cr_3AlB_4, and Cr_4AlB_6: the first members of the series $(CrB_2)_nCrAl$ with n=1, 2, 3 and a unifying concept for ternary borides as MAB-phases, Inorg. Chem. 54 (13) (2015) 6122–6135.
[89] P. Eklund, J. Rosen, P.O.A. Persson, Layered ternary $M_{(n+1)}AX_{(n)}$ phases and their 2D derivative MXene: an overview from a thin-film perspective, J. Phys. D. Appl. Phys. 50 (11) (2017).
[90] W. Rieger, H. Nowotny, F. Benesovs, Uber einige komplexboride von ubergangs-metallen, Mon. Chem. 96 (3) (1965) 844–851.
[91] X.H. Li, H.L. Cui, R.Z. Zhang, First-principles study of the electronic and optical properties of a new metallic MoAlB, Sci. Rep. 6 (2016).
[92] S. Kota, E. Zapata-Solvas, A. Ly, J. Lu, O. Elkassabany, A. Huon, W.E. Lee, L. Hultman, S.J. May, M.W. Barsoum, Synthesis and characterization of an alumina forming nanolaminated boride: moaib (vol 6, 26475, 2016), Sci. Rep. 6 (2016), 2016.
[93] M. Naguib, M. Kurtoglu, V. Presser, J. Lu, J.J. Niu, M. Heon, L. Hultman, Y. Gogotsi, M.W. Barsoum, Two-dimensional nanocrystals produced by exfoliation of Ti_3AlC_2, Adv. Mater. 23 (37) (2011) 4248–4253.
[94] L.T. Alameda, P. Moradifar, Z.P. Metzger, N. Alem, R.E. Schaak, Topochemical deintercalation of Al from MoAlB: stepwise etching pathway, layered intergrowth structures, and two-dimensional MBene, J. Am. Chem. Soc. 140 (28) (2018) 8833–8840.
[95] V. Ivanchenko, T. Pryadko, Boron – iron – titanium, in: G. Effenberg, S. Ilyenko (Eds.), Iron Systems, Part 1: Selected Systems From Al-B-Fe to C-Co-Fe, Springer Berlin Heidelberg, Berlin, Heidelberg, 2008, pp. 544–556.
[96] C. Kapfenberger, B. Albert, R. Pottgen, H. Huppertz, Structure refinements of iron borides Fe_2B and FeB, Z. Kristallogr. 221 (2006) 477–481.
[97] R.M. Minyaev, R. Hoffmann, Transition-metal borides with the Ta3b4 crystal-structure - their electronic and bonding properties, Chem. Mater. 3 (3) (1991) 547–557.
[98] Y.B. Kuz'ma, P.I. Krypyakevych, M.V. Chepiga, Crystal structures of the compounds MoCoB, WCoB, and WFeB, J. Struct. Chem. 9 (1968) 268–269.
[99] M.V. Chepiga, Y.B. Kuz'ma, The system rhenium-cobalt-boron, Inorg. Mater. 9 (1973) 1505–1511.